NASA Contractor Report 198467
AIAA–96–1718

# An Experimental Investigation of Screech Noise Generation

J. Panda
*Modern Technologies Corporation*
*Middleburg Heights, Ohio*

April 1996

Prepared for
Lewis Research Center
Under Contract NAS3–27377


National Aeronautics and
Space Administration

# AN EXPERIMENTAL INVESTIGATION OF SCREECH NOISE GENERATION

J. Panda*
Modern Technologies Corporation
Middleburg Heights, Ohio 44130

**Abstract**

The screech noise generation process from supersonic underexpanded jets, issuing from a sonic nozzle at pressure ratios of 2.4 and 3.3 (fully expanded Mach number, $M_j = 1.19$ and 1.42), was investigated experimentally. Spark schlieren visualization at different phases of the screech cycle clearly shows the convection of the organized turbulent structures, and the associated hydrodynamic pressure field, over a train of shock waves. The rms pressure fluctuation at the screech frequency was measured in the nearfield region by a traversing microphone. The data show the presence of two sets of interconnected peak and valley patterns: one along the jet boundary and the other along a diagonal direction. Both of these patterns are shown to be an outcome of a standing wave formation between the upstream propagating acoustic and downstream propagating hydrodynamic fluctuations. Laser light scattering by turbulence was utilized to measure convective velocity of the organized structures. The convective velocity is found to change periodically from subsonic to supersonic values with respect to the ambient sound speed. Interestingly, the periodicity is found to be the same as that of the standing wave spacing. For the present experimental conditions, the standing wave spacing is smaller than the shock wave spacing. An analysis of data obtained by Raman and Rice (1994) and Hu and McLaughlin (1990) reveals that the turbulent fluctuations are also modulated periodically at the standing wave spacing expected in their facilities. It is demonstrated that the existing screech frequency formulae can be derived from the simple standing wave relationship between the acoustic and the hydrodynamic fields. Based on the above observations and additional support from the supersonic wavy wall analogy, it is proposed that there exist multiple sound sources, equispaced by a standing wavelength, in the jet shear layer. The time evolution of the pressure fluctuations over the nearfield region was obtained from phase averaged microphone measurements. An analysis of this data further clarifies the sound generation process. The coherent hydrodynamic fluctuations are identifiable within a short distance from the jet boundary. They have a short wavelength, propagate downstream with the flow and, their amplitude is modulated periodically with the standing wave spacing. The relatively weak and longer wavelength acoustic fluctuations are found to originate from the hydrodynamic fluctuations. By following an upstream propagating acoustic wave, it is found that the source of the compression or the rarefaction part is a similar hydrodynamic fluctuation lying approximately between the 3rd and the 4th shock. Subsequently, the acoustic wave propagates in a curious pause-and-go, walking motion over the modulated hydrodynamic field. Such interactions further strengthen the acoustic wave.

## I. Introduction

Screech noise is produced by incorrectly expanded supersonic jets issuing from nozzles of regular geometry. The characteristic discrete tones can be heard from over and underexpanded supersonic jets. When present, the sound level associated with the screech tone dominates over all other jet noise components in the forward direction[1] (upstream of the nozzle exit). Seiner, Manning and Ponton[2] studied twin-jet screech resonance with nozzle geometries found in military aircraft and measured very high dynamic loads capable of causing tailplane structural failure. In an earlier study Hay and Rose[3] also had made similar observation. This provides, in part, the motivation for the current work. The goal is to provide a knowledge base and a data base which can be used along with computational methods[4] to predict the frequency and amplitude of the screech tone.

The overall, self-sustaining, feedback loop that controls the screech production mechanism has been explained by Powell.[5] Since then there have been many visualization[6,7,8] and other experimental studies[9-13] to validate the mechanism. In his screech directivity model, Powell placed 3 to 4 sources at the shock locations along the jet boundary

*NASA Resident Research Associate at Lewis Research Center, Cleveland, Ohio 44135 Member, AIAA. voice: 216-433-8891, email: panda@yaz.lerc.nasa.gov

with a fixed phase relation between the individual sources.[14] This simple model is found to capture the farfield directivity quite accurately, as confirmed by Norum.[15] It was believed that the oscillation of the shock system produces sound which, perhaps, prompted the decision to place the sound sources at the shock location for the purpose of modelling. The next step in the buildup of the current understanding of screech is the relationship between it and the shock associated broadband noise.[16,17] Fisher and Morfey[16] have demonstrated that the screech frequency is a special case of shock-associated broadband noise when the observation angle is at 180° with the flow direction. From an analysis of frequency spectra, Tam *et al.*[17] showed that the frequency spread of the broadband shock associated noise decreases and the center frequency approaches the screech frequency as the observation angle approaches 180°. The screech frequencies predicted by various models (Powell, Fisher-Morfey and Tam *et al.*) are somewhat close to the actual measured value, although none are able to predict the sudden jump in frequency, known as mode switching.[15] Later on, Morris *et al.*[18] have used the above ideas to approximately predict the screech frequencies of non-circular, arbitrary geometry jets. Another important, and still unsolved part of the problem is in predicting the amplitude of the screech tone, for which none of the above models provides any clue.

It is believed that the above inabilities are due to a void in our understanding of many physical processes involved in the overall feedback loop. Some of the unresolved questions are: How do the turbulent structures interact with shocks to create sound? Where do the effective sound sources exist? How do the shocks respond to a periodic train of disturbances and how do the sound waves generate more periodic disturbances in the flow (the receptivity problem)?

An experimental program has been undertaken at NASA Lewis Research Center to answer some of the above questions. A detailed study of the shock shapes and their motion in the plume of a circular, underexpanded, supersonic jet has been presented earlier.[19,20] The present paper addresses the issue of source identification and the mechanism of sound generation from a combined action of multiple sources. The experimental conditions are identical to the ones used in the earlier work.

Experimental data presented in this paper were obtained from either the jet shear layer or the extreme nearfield region that extends radially from just outside the shear layer to about 7 diameters away from the centerline. The experimental techniques used for this study are non-intrusive in nature: microphone traverses outside the flow, laser light scattering by turbulence, and schlieren visualization. Detailed phase averaged measurements and schlieren photography were conducted to unveil the unsteady processes. The consequences of the new experimental findings on our understanding of the screech generation process are discussed in the last section, summary and conclusion.

There have been many experimental studies to determine the sources of screech noise;[5,9,10,21] the unanimous agreement is that there are more than one source that lie somewhere between the second and the fifth shock. However, the reason for such positioning of the sources is not evident. A good set of data obtained by Hu and McLaughlin[22] from a low Reynolds number jet experiment provides some clue. These are discussed in the paper. Most of the earlier experimental work have concentrated on time averaged measurements, while the sound generation process is a time-dependent one. A notable exception is a series of innovative experimental studies by Westley and Wooley,[11–13] who had measured time varying fluctuating pressures using analog instruments. Some observations made in these earlier studies have been duplicated in the present work, which makes extensive use of digital computers and analyzers. The primary problem with the above studies is a limited phase resolution and a limited analysis of the experimental data. The limited phase resolution has obscured a significant amount of physics which is described in detail in this paper.

## II. Experimental Setup

The present experiments were conducted in a free air jet facility at the NASA Lewis Research Center (Fig. 1). A 25.4 mm diameter (D) axisymmetric, convergent nozzle is used to produce underexpanded supersonic jets which, if fully expanded, would have Mach numbers ($M_j$) in the range 1.1 to 1.65. The Mach number range was achieved by changing the supply pressure to the plenum chamber.

The experimental data reported herein were obtained using nonintrusive techniques. Since, it is well-known that the screech is sensitive to the presence of any sound reflectors in the vicinity of the jet, all such objects were wrapped by polyurethane foam to avoid strong reflection. Even when a probe or an optical element was placed close to the jet especial attention was given not to change the screech frequency. The primary reflector that has helped to produce a steady and a large amplitude screech noise is the metallic nozzle block itself, detail of which is shown in Fig. 1(b). The 305 mm diameter flange is found to be the major source of reflection. This was established by selectively covering individual surfaces with polyurethane foam. Both the screech amplitude and frequency can be changed by partly or fully covering the flange.

The screech tone frequencies and circumferential mode shapes have been measured for the above Mach number range and have been presented in an earlier publication.[19] The present experiments were conducted for two operating conditions, for which the fully expanded jet Mach numbers ($M_j$), screech frequencies and screech modes are respectively, 1.19, 8400 Hz, axisymmetric, and, 1.42, 5400 Hz, helical. The operating conditions were selected based on the availability of a stable screech tone. This is essential for an accurate phase averaged measurement.[19]

The flowfield was visualized by a standard schlieren system using two 152 mm diameter and 914 mm focal length spherical mirrors. A spark source that provides enough light in about a microsecond duration was used to freeze the flow. The knife edge position is vertical; therefore, the horizontal density gradient is visible in all photographs presented in this paper. Light from the knife edge is allowed to fall directly on a Nikon F4 camera. The camera shutter was kept open and the light source was externally triggered to obtain a single image. To produce multiple light flashes at a given phase of the screech cycle a special triggering mechanism was built. The mechanism operated on a reference screech signal from a fixed microphone placed upstream of the nozzle exit. An adjustable delay generator and a single-pulse-capturing circuit provided the trigger signal necessary to close the spark gap of the light source. For phase averaged photographs, the camera shutter was kept open and the film was exposed to six flashes at the same phase of the screech cycle.

The convective speed of the organized turbulent structures was measured by an optical method involving a narrow pencil of laser beam passing through the shear layer and normal to the flow direction. The refractive index fluctuations associated with the density fluctuation of the passing eddies cause light scattering within a narrow angle with respect to the beam propagation direction.[23,24] This scattered light was collected and measured by a photomultiplier tube (PMT).

The optical arrangement, shown in Fig. 2, is the same as used earlier to collect light scattered from shock waves.[19,20] A green (0.514 mm wavelength) laser beam, separated from an Argon-ion laser and transmitted through a fiber optic system, is the central element. The 2mm diameter laser beam coming out of the fiber-optic probe is focused to a 0.16 mm spot at the jet centerline and is allowed to cross the flowfield. On the other side of the jet is a light collecting and measuring device which senses the scattered light. There are a beam stop and an aperture stop just in front of the 60 mm diameter collecting lens. The diameter of the beam stop is such that the main laser beam is blocked from entering the collecting optics while the scattered light can be easily collected. The collecting lens passes this light to a photomultiplier tube (PMT) via a pinhole. The electrical output from the PMT is connected across a 50 Ω terminator (not shown in Fig. 2). The voltage drop across the terminator is proportional to the PMT current and, therefore, is an indicator of the intensity of the collected light.

The complete optical set-up (fiber-optic probe, beam stop and the collecting optics) was mounted on a traversing unit (Klinger) which allowed it to be positioned at various points along the jet shear layer. Under no flow condition, light from the laser beam does not reach the PMT. However, the scattered light produced by the refractive index fluctuation in the flow is collected and sensed as a non-zero voltage output. It has been already mentioned that the same system was used to measure light scattered by shock waves present in the jet. However, the shocks are present at a few discrete regions, and the PMT signal level is nearly 3 orders of magnitude higher than that from the refractive index fluctuations alone. Therefore, it was somewhat straightforward to discriminate scattering signatures of organized structures from those of the shock waves. A voltage threshold level was established and PMT output above this level are considered due to light scattering by the shock. Such data are not presented in this paper.

The voltage signal from the PMT, as well as all other voltage outputs from various measuring devices were digitized using a dsp Technology sample-and-hold digital converter and then stored and processed by a Microvax 3300 computer.

There are a few implicit assumptions made throughout the text which should be mentioned at the outset. The shock locations, indicated in the figures, correspond to their position in the jet shear layer. It has been pointed out in Ref. 19, that the shocks move most in the jet core and least in the shear layer. Another assumption is in the use of the term 'jet boundary.' Strictly speaking, the radial boundary of the jet flow lies at infinity as the primary jet flow induces an entrainment motion in the ambient fluid. For the present work, however, jet boundary refers to the boundary of the turbulent motion from the primary jet, as visible in a schlieren photograph. It is estimated that, on an average, the initial shear layer spreading is limited within a 5.7° angle with respect to the flow direction. A straight line drawn from the nozzle lip at the above angle is referred to the jet boundary in this paper.

## III. Results

### A. Visualization of shock/organized structure interaction

Figure 3 presents a set of 12 spark schlieren photographs over a screech cycle for the $M_j = 1.19$ jet. The constant value of phase difference between the successive photographs is 30° ($\Delta\tau/T = 0.083$, where $\tau$ is the phase time, and T is the time period of screech). Each photograph shows multiple dark regions corresponding to the high density compression zones and, in between, lighter regions corresponding to the low density expansion zones. An examination of the darker regions from frame to frame reveals two sets of periodic structures. One set is somewhat fixed in space and the other is convecting downstream. The fixed ones are the shock waves shown by vertical arrows in Fig. 3(a), and the convecting ones correspond to the high density sides of organized turbulent eddies. Perhaps the best way to discriminate the two is by comparing the instantaneous photographs with a time averaged photograph. The latter one averages out signatures of the convecting structures and leaves the footprints of shocks. Such a time averaged photograph is shown later (Fig. 5(b)). The vertical arrows of Fig. 3(a), indicating shock boundaries in the jet shear layer, are obtained from such a comparison. In three dimensions the shock waves are imbedded in the jet core and have a conical or disk-like shape,[19] while the organized turbulent structures are present in the jet periphery and are of doughnut shape. There are 3 to 4 axisymmetric organized structures in each photograph which are convecting over the shock train as the phase time progresses. The vertical and slightly inclined dashed line connects one such organized structure from frame to frame and portrays the convection process. The distance moved by each structure in a screech cycle is one wavelength ($\lambda_h$), which is also the spacing between two such consecutive structures in each photograph.

A noticeable feature is a considerable loss of coherence of the organized structures as they propagate beyond about four jet diameters (5th shock) from the nozzle exit. The small markers at the bottom of each photograph are one jet diameter apart and a downstream distance of about 5 diameters is visible in each photograph. The organized structures are found to grow up to the second shock; they are most pronounced between the second and the fifth shock, after which they start to loose coherence.

It was estimated that there exist a random phase error of ±15° about the preset phase time in firing the spark unit. The phase time of the photographs of Fig. 3 is accurate within this error. In addition, there are certain other uncertainties inherent to a set of single exposure images. There is a long time gap between the individual images, and the appearances of the organized structures are different from photograph to photograph due to their natural differences and jitter in position. Note that the shock waves also oscillate about their mean positions.[19] Such a motion, however, is difficult to see in Fig. 3.

Phase averaged schlieren photographs

The jitter and cycle-to-cycle difference in the schlieren photographs of Fig. 3 are somewhat averaged out in the multiple-exposure (six) phase averaged photographs of Fig. 4. Note that Fig. 4 shows photographs of the $M_j = 1.42$ jet which produces screech in a helical mode, while figure 3 corresponds to the lower $M_j = 1.19$ jet where screech tone is in an axisymmetric mode. The helical screech mode implies that the organized turbulent structures also have the same helical azimuthal shape. This is somewhat clear at the right edge of the photographs. The axisymmetric shock waves are distinctly separable from the organized structures. Another major difference is produced by a larger knife edge cutoff that has made a more sensitive schlieren arrangement. The higher schlieren sensitivity has accentuated an additional feature: the nearfield pressure fluctuation outside the jet flow boundary.

The jet flowfield is marked by a plethora of tiny bright and dark grains left by the random turbulent fluctuations. The darker, higher density sides of the organized structures are found to extend beyond the jet boundary into the very nearfield region. Such extensions are the footprints of compression zones associated with hydrodynamic and acoustic waves. One problem with the phase averaged photographs is a loss of sensitivity at the right edge, which prohibits visualization of the nearfield pressure fluctuations beyond about three jet diameters. The large knife edge cut off has accentuated the small optical coma at the second focal point of the schlieren set-up and is believed to be the reason for the nonuniformity.

In spite of the above problem a curious merging process between two adjacent compression waves becomes apparent in Figs. 4(c) to (g). A weak (upstream) and a strong (downstream) compression zone at the top half of the jet in Fig. 4(c) (indicated by two vertical arrows) are found to go through a merging process that ultimately resulted in an exchange of energy to the upstream zone. It will be shown later in the paper that this is the process by which the downstream propagating hydrodynamic field transfers energy to the upstream propagating acoustic waves.

### B. Time averaged data

Figure 5 shows schlieren photographs of the jets and the rms value of the fluctuating pressure measured in the nearfield using a traversing microphone. Each schlieren

photograph was obtained by exposing a single negative to eight random flashes which, in effect, produced a time-averaged view of the flowfield. The darker regions represent shock compression and the brighter ones expansion zones. The sharp vertical boundary at the end of each compression zone corresponds to the termination position of each shock in the shear layer around the jet.

The root-mean-square of the fluctuating pressure at the screech frequency is expressed in the standard decibel scale (reference level = $2\times10^{-5}$ Pa). Such data were obtained from narrow-band frequency spectra. The spectral levels at the screech frequency are plotted in this figure. The 3.18 mm microphone was traversed from point to point over a grid of 53 axial by 19 radial positions for the $M_j = 1.42$ case, and 51 axial by 21 radial for the $M_j = 1.19$ case. The grid spacing is uniform in the axial direction (0.15D for $M_j = 1.42$ and 0.12D for $M_j = 1.19$ jets) and is progressively increased from 0.2 to 0.4 D in the radial direction. This has provided about 16 (closest to the jet boundary) to 5 (farthest from the boundary) points per acoustic wavelength, which is deemed to be sufficient to resolve the pressure fluctuations. To avoid damaging the fragile microphone diaphragm from direct impingement of the jet flow, traverses were made outside the flow boundary. The 5.7° angle with respect to the jet axis, visible at the lower edge of each color plot, was chosen to account for the jet spread in the downstream direction. The color bar of Fig. 5 has two sets of levels. The levels on the left are used to plot $M_j = 1.19$ data (top plot) and those on the right for $M_j = 1.42$ data (bottom plot). The fluctuating pressure levels, shown in these plots, have contributions from the acoustic waves radiated by the jet as well as the hydrodynamic pressure field of the passing organized structures in the shear layer. This will be especially clear from the later discussion.

The time averaged fluctuating pressure field is quite complex. The overall appearance, however, is similar for the two cases presented in this figure. There are two sets of periodic patterns visible in each color plot: the red-yellow pattern along the jet boundary, and the red-blue pattern along a diagonal. The axisymmetric nature of the flowfield implies that in three dimensions the patterns are wrapped around the jet. Similar experimental data and periodic patterns were also presented by Westley and Wooley[11,12] for an axisymmetric jet and Rice and Taghavi[9] for a rectangular jet. Out of the two patterns, the red-yellow one along the jet boundary is considered first. The rms value of the pressure fluctuations differ by 20 dB between the yellow (crest) and red (trough) regions. A comparison with the schlieren photographs show that there is a small mismatch between the shock spacing (L) and the spacing between the crests ($L_p$). In general, crests lie in between two adjacent shock tips. There are, however, visible exceptions; the pressure crest just over the first shock in Fig. 5(c) is an example.

From an examination of the various wavelengths involved, it can be shown that the maxima and the minima in the pressure fluctuations are due to a standing wave formation between the downstream propagating hydrodynamic and the upstream propagating acoustic fluctuations. The wavelengths of hydrodynamic pressure fluctuation are measured from the phase averaged data presented later in the paper. If we consider two oppositely moving wave systems of the same frequency, $\omega$, and different wavelengths $\lambda_s$ and $\lambda_h$, the resultant fluctuation can be written as:

$$f = \sin\left(\frac{2\pi}{\lambda_s}x + \omega t\right) + \sin\left(\frac{2\pi}{\lambda_h}x - \omega t\right) \qquad (1)$$

The mean-square of the resultant fluctuation is calculated as:

$$\bar{f}^2 = \frac{\omega}{2\pi}\int_0^{\frac{2\pi}{\omega}} f^2 dt = 1 - \cos 2\pi\left(\frac{1}{\lambda_s} + \frac{1}{\lambda_h}\right)x.$$

The above equation shows that a standing wave pattern is expected with a spatial periodicity $L_{sw}$ that satisfies

$$\frac{1}{L_{sw}} = \frac{1}{\lambda_s} + \frac{1}{\lambda_h}. \qquad (2)$$

Table I demonstrates that, if $\lambda_s$ and $\lambda_h$ are assigned to the sound and hydrodynamic wavelengths, respectively, the spacing between the neighboring crests ($L_p$) follows the above equation, i.e., $L_p = L_{sw}$. In the past, Rice and Taghavi,[9] and Tam[1] have also attributed the crest and troughs to a standing wave formation. It should be mentioned here that only a partial standing wave formation is expected. The primary reason is an amplitude mismatch between the two wave systems involved. Along the jet boundary, the hydrodynamic fluctuations are found to be an order of magnitude higher than the acoustic one. However, the hydrodynamic fluctuations decay exponentially away from the jet boundary,[25] this makes the acoustic fluctuations dominate after a certain radial distance.

It is interesting to note that an identical expression for the screech frequency, obtained by Powell[5] from the consideration of a feedback loop, and by Fisher and Morfey[16] from a consideration of the upstream directivity of a phased array of acoustic sources, can also be obtained from Eq. (2). Since, $\lambda_s = c/f_s$, and $\lambda_h = u_c/f_s$, (where c is the ambient sound speed, $f_s$ is the screech frequency, and $u_c$ is the convective speed of hydrodynamic fluctuations) Eq. (2) can be written as:

$$\frac{1}{L_{sw}} = \frac{f_s}{c} + \frac{f_s}{u_c}.$$

Rearranging,

$$f_s = \frac{u_c}{L_{sw}\left(1 + \frac{u_c}{c}\right)} \tag{3}$$

Equation (3) provides an exact expression for screech frequency. An approximate expression is obtained if the wavelength of the standing wave is equated to the shock spacing, $L_{sw} \sim L$.

$$f_s = \frac{u_c}{L(1+M_c)}, \tag{4}$$

where, $M_c$ is the convective Mach number, $u_c/c$. Equation (4) is identical to the relationship obtained by Powell[5] and Fisher and Morfey.[16] The screech frequency formula provided by Tam *et al.*[17] can also be obtained from Eq. (3). Tam *et al.* assumes that the convective velocity of the hydrodynamic fluctuations is 70 percent of that the fully expanded jet velocity ($u_j$), i.e., $u_c = 0.7\,u_j$. Using isentropic relationships to relate $u_j$, and sound speed c, to the reservoir temperature $T_r$, ambient temperature $T_a$, and the fully expanded jet Mach number $M_j$, Eq. (3) can be written as:

$$f_s = \frac{0.7u_j}{L_{sw}}\left[1 + 0.7M_j\left(1 + \frac{\gamma-1}{2}M_j^2\right)^{-\frac{1}{2}}\left(\frac{T_r}{T_a}\right)^{\frac{1}{2}}\right]^{-1}. \tag{5}$$

For a circular jet, Tam *et al.* has used 80 percent of the shock cell spacing to derive the empirical relation. Interestingly, it can be seen from Table I that the standing wave spacing, $L_{sw}$ (= $L_p$) is approximately 80 percent of the average shock spacing. The Prandtl-Pack[26] formula provides the necessary relationship between the shock spacing and $M_j$ :

$$L_{sw} \approx 0.8L = 0.8\left[1.306\left(M_j^2 - 1\right)^{\frac{1}{2}}D\right]. \tag{6}$$

Combining Eqs. (5) and (6):

$$\frac{f_s D}{u_j} = \frac{0.67}{\left(M_j^2-1\right)^{\frac{1}{2}}}\left[1 + 0.7M_j\left(1 + \frac{\gamma-1}{2}M_j^2\right)^{-\frac{1}{2}}\left(\frac{T_r}{T_a}\right)^{\frac{1}{2}}\right]^{-1}. \tag{7}$$

Equation (7) is the same as that of Tam *et al.*, except for a minor replacement of fully expanded jet diameter, $D_j$, by the physical jet diameter D. The underlaying point in the above discussion is that a standing wave formation is essential to generate screech noise and all known formulae of the screech frequency can be rewritten as a condition for such a formation. Additional data presented in the next sections raise a possibility that the standing wave spacing is inherent to an underexpanded jet and the screech frequency is selected to satisfy the above.

The diagonal red-blue pattern seen in Figs. 5(a) and (c) is found to be related to the red-yellow standing wave pattern along the jet boundary. This is demonstrated in Fig. 6, which is a noncolor version of Fig. 5(c) with additional contours at a finer level. An almost parallel set of curved lines can be drawn through the local maxima in the contours lying between the jet boundary and a 39° diagonal line. The latter joins the diagonal red-blue pattern. The spatial periodicity ($L_b$) is measured to be 1.02D, which is equal to the projection of the standing wave periodicity ($L_{sw}$) along the jet boundary onto the diagonal line. In other words,

$$L_b = L_{sw}\cos\theta; \quad \theta = 39°. \tag{8}$$

This is somewhat expected, as along an oblique line, that makes an angle θ with the upstream direction, the standing wave spacing is given by:

$$\frac{1}{L_b} = \frac{1}{\lambda_s/\cos\theta} + \frac{1}{\lambda_h/\cos\theta} \tag{9}$$

which simplifies to Eq. (8). This discussion points out that the standing wave formation is not limited to the jet boundary, it permeates over a larger nearfield region. Following is a discussion of the screech harmonics.

Figure 7 shows fluctuating pressure levels close to the jet boundary, similar to Fig. 5, but for the harmonic of screech frequency. To clarify the directivity patterns, equipressure contour levels are plotted for pressure fluctuations above 127 dB (Fig. 7(a)) and 140 dB (Fig. 7(b)). There are two distinct beams of sound at 90°, and about 120° to the jet axis. The angles are measured from the jet flow direction. The normal beam is relatively stronger for the $M_j$ = 1.42 jet (Fig. 7(b)) and the forward propagating one is stronger for the $M_j$ = 1.19 jet (Fig. 7(a)). An examination of the contour levels shows that the pressure amplitude decreases progressively away from the jet boundary. Once again, close to the jet boundary, there are indications of standing wave formation; however,

the spacings are shorter and correspond to a linear superposition of harmonic frequency waves. All of these show that the screech harmonic is primarily generated by the flow. Some additional support is found in the experimental data of Walker *et al.*[27] and Raman and Rice,[28] who have measured considerable velocity fluctuations at the harmonic frequencies inside the jet shear layer. The propagation nonlinearity of the fundamental tone may play only a secondary role.†

### C. Unsteady measurements of nearfield pressure fluctuations

The phase averaged pressure fluctuation measurements, shown in Fig. 8, were obtained over the same grid points as discussed earlier in connection with the time averaged data. The signal from a microphone placed upstream of the nozzle was used as a reference for the phase averaged measurements. To produce a repeatable phase reference, the reference microphone signal was band-pass filtered about the fundamental screech frequency. This eliminated the broadband noise components. (The same signal was also used for phase reference of the schlieren photographs). A 3.18 mm diameter microphone was traversed from point to point in the flowfield and, at every measurement station the pressure signal, p{t, x/D, r/D}, was phase averaged over more than 100 screech cycles to obtain <p>{ τ/T, x/D, r/D}. The data were stored in the Microvax computer for later processing.

Following is a discussion on the measurement accuracy. The complete data set was repeated three times; twice using a 3.18 mm diameter microphone and once using a 6.35 mm diameter microphone. The pressure fluctuation values are found to be closely repeatable. The only major discrepancy appears in the absolute magnitude close to the jet boundary where a ±5 percent difference is not uncommon. This is somewhat expected as the rms level along the jet boundary crosses the dynamic range of the microphone: 165 dB. The spatial resolution to which the pressure fluctuations can be resolved is not a problem except close to the jet boundary where a change of 20 dB can occur over a distance of 0.7D (17.8 mm, Fig. 5(a)). The 3.18 mm diameter microphone introduces some spatial averaging over the area covered by the sensor diaphragm. The temporal resolution is limited by the sampling rate in the analog-to-digital converter used to acquire the microphone signals. A sampling rate of 200,000/s and a screech frequency of 8400 Hz provided about 24 data points per cycle. This translates into a phase uncertainty of ±8°. Another concern, that finally limits the measurement accuracy, is the fluctuating plenum pressure which also changes the screech frequency. The compressed air was supplied from a central facility which feeds many other test installations. Therefore, a certain amount of fluctuation was unavoidable. However, the plenum pressure, measured using a Setra pressure transducer, was continuously monitored and the data acquisition was performed only when it remained within ±0.5 percent of the desired setting. The accompanying drift in screech frequency was ±25 Hz This condition was imposed for all data presented in this paper.

Each multicolor plot of Fig. 8 shows a set of compression (above ambient, red-yellow) and rarefaction (below ambient, blue-green) regions which move in a complicated fashion as the phase time progresses. The instantaneous pressure levels at every measurement station are the resultant of hydrodynamic and acoustic fluctuations. It is impossible to isolate individual contributions as both are in the same frequency. Moreover, a standing wave is formed between the two. Nevertheless, a careful examination reveals many interesting features which can be attributed primarily to hydrodynamic or to acoustic waves. Note that the measurement region covers more than 8 shock cell spacings from the nozzle exit. It is known from earlier schlieren visualization[5,6,8] that the screech waves are generated within the fifth shock from the nozzle exit. Therefore, the region covered by the experimental data should show not only a simple interaction between the hydrodynamic and the acoustic fluctuations but also the generation of the latter. It is discussed later in the paper that the standing wave can be thought of as a cause rather than an effect of sound generation.

A complete wave is made of a compression and a rarefaction zone; therefore, a wavelength is the distance covered by two such adjacent zones. By following the motion of different such zones, from plot to plot, one can see the presence of two types of waves. The relatively smaller wavelength ones lying next to the jet boundary, and having a high level of pressure fluctuations (green and deep red), are found to propagate downstream with the flow. Such waves are marked by the arrow I in Fig. 8(a) and are identifiable within a radial distance from the bottom boundary of each color plot. These are primarily associated with the hydrodynamic pressure fluctuation from large organized structures. The pressure maxima and minima associated with the hydrodynamic waves are very high. Some contour levels in such extreme regions close to the jet boundary are not drawn in Fig. 8 for the sake of clarity. The second type of waves occupy most of the measurement region. They have a larger wavelength, and

†For the first reading, it may be fruitful to jump section C and continue with section D.

are relatively weak (blue and pale red). They are present above the hydrodynamic waves and are found to propagate either upstream or downstream depending on their point of origin. These are identified primarily as the sound waves.

The nature of the hydrodynamic waves becomes particularly clear from a combined view of the flowfield and the nearfield pressure fluctuations. This is shown in Fig. 9 where the instantaneous pressure fluctuation data are superimposed on the phase averaged schlieren photographs, obtained at identical phase times. The multicolor pressure fluctuation plots are the same as shown in Fig. 8. The phase averaged, multiple-exposure (six) schlieren photographs are somewhat similar to the single exposure ones shown earlier in Fig. 3. Like before, two trains of periodic dark patterns, the spatially fixed shock waves and the downstream convecting organized turbulent eddies, are also visible in the schlieren photographs. The connection between the microphone data and the schlieren photographs is made through the hydrodynamic compression zones, which manifest as darker regions beyond the jet boundary in the schlieren photographs, and the deep red regions along the lower boundary of the microphone data. Since, the phase averaged microphone data and the schlieren photographs were obtained using identical trigger signals, phase matching was straightforward. Figure 9 demonstrates the radial penetration of hydrodynamic pressure fluctuations into the quiescent ambient air. It also confirms that the red-green regions, along the bottom boundary of each multicolored plot, correspond to the hydrodynamic pressure fluctuations.

Returning back to the Fig. 8(a), the propagation direction of the acoustic waves are shown by arrows II and III. The bases of the arrows lie in a demarcation region. All sound waves lying right of this region propagate downstream, while the rest propagate upstream. The blue-green rarefaction region that lies in the demarcation zone, and is marked by a star in Fig. 8(a) shows a special behavior not found in others. The initial hydrodynamic fluctuation is found to produce a weaker rarefaction zone of length scale compatible to the acoustic wave. This is believed to be the source of the acoustic fluctuation from the hydro-dynamic field. The demarcation region lies nominally between the third and the fourth shock ($2.37 < x/D < 3.07$) and the development of the acoustic fluctuations occur as the boundary of a compression or a rarefaction part of a passing hydrodynamic wave bulges out radially. A phase difference of half a cycle is maintained between the inception of the compression and the rarefaction part. In the following the development and growth of the rarefaction part alone is described.

The progressive development of the rarefaction zone, shown by a star in Fig. 8(a), is traced in Fig. 10 where the same experimental data are plotted using the same contour levels, but without any color. The phase time of each plot of Fig. 10 is the same as that shown in Fig. 8. The only exceptions are Fig. 10(c) and (i). The former is added to make the sudden changes between 8(c) and (d) legible and the latter to show the net change over a screech cycle. The rarefaction zone of Fig. 10(a) is observed to bulge out radially, away from the jet boundary, to a size that corresponds to the half wavelength of the screech waves (Fig. 10(b)). It then shears off into two parts (Fig. 10(c)): the upper half, with a length scale corresponding to the sound wave, moves upstream while the lower half, associated with the hydrodynamic field, continues its journey in the downstream direction. In between Figs. 10(c) and (e), the acoustic wave jumps over a dissimilar region associated with the hydrodynamic fluctuation and becomes attached to the similar region from the upcoming fluctuation. The process of repulsion between the dissimilar regions and attraction between the similar regions is performed two more times in the right half of Fig. 10. A video animation of all data sets (24 frames covering a screech cycle) shows this motion very clearly. The compression or the rarefaction part of an acoustic wave is found to dwell on the similar part of a hydrodynamic wave for a relatively longer time and quickly jump over a dissimilar part. The resulting movement has a curious "pause-and-go" feature that is very different from a steady wave propagation.

Figure 10(i) is at the same phase time as 10(a); the only difference is that a complete screech cycle has passed in between. The original rarefaction part of the hydrodynamic wave has moved to the right most edge (shown by a star), while a fully formed acoustic wave is approaching the nozzle exit. Notice that a new acoustic wave is developing between the 3rd and 4th shock. Clearly, the fully formed acoustic wave is far stronger than the one at inception. The required energy transfer from the hydrodynamic to the acoustic wave has occurred during the interaction processes depicted between Figs. 10(b) and (h). A closer examination of the changes in the contour levels reveals that the rarefaction part of a sound wave becomes slightly weaker when passing over a dissimilar region of a hydrodynamic fluctuation, however, the loss is more than compensated for when the similar regions of the acoustic and the hydrodynamic fluctuations interact. Therefore, the hydrodynamic field not only acts as a source but also nurtures the growth of the acoustic field.

Figure 10 describes the dynamics of the rarefaction part of a sound wave. The complimentary compression part

also develops between the 3rd and the 4th shocks in Fig. 8(e) and can be found to follow the same dynamics described above.

An additional set of data showing the sound generation and propagation process for the $M_j = 1.42$ jet was acquired. The fundamental dynamics of the acoustic and the hydrodynamic waves are found to be the same as described above.

The "pause-and-go" feature and the amplitude modulation of the acoustic waves are telltale signs of a partially formed standing wave. The video animation, mentioned earlier, shows modulations of the hydrodynamic field also. An attempt to graphically demonstrate this feature is made in the following.

Amplitude modulation of pressure fluctuations along jet boundary

The pressure field lying in the immediate neighborhood of the jet boundary is found to be considerably modulated. This is an expected consequence of the standing wave formation. However, amplitude modulation of a propagating fluctuation due to a super-imposed standing wave, is not as vivid anywhere else as in Fig. 11. The phase averaged pressure fluctuations data along the bottom boundary of the measurement region is plotted in Figs. 11(a) and (c), and the root-mean-square values obtained from the identical measurement stations are shown in Figs. 11(b) and (d). Data obtained for both the $M_j = 1.19$ and 1.42 jets are shown in this figure. Note that the microphone traverses were made at an oblique angle to the jet axis. The microphone was closest to the jet at the nozzle lip (r/D = 0.6 and 0.7 for respectively $M_j = 1.19$ and 1.42 jets) and was traversed at an angle of 5.71° to the jet axis. This was necessary to avoid damaging the sensor diaphragm from direct impingement of the jet fluid and to account for the progressive growth of the jet boundary.

To highlight the amplitude modulation process, double sided arrows, indicating the maximum compression (Fig. 11(a)) or rarefaction (Fig. 11(c)) associated with two waves, are shown. The standing wave spacing is about one half of the hydrodynamic wavelength. Therefore, the pressure levels associated with one half of the hydrodynamic wave are indicated. One can also follow a complementary part and conclude that the spatial position where the rarefaction part grows is where the compression part also grows. There exists one half of a cycle phase time difference between the two. A comparison between the phase averaged and rms data shows that the locations of local maxima in the rms pressure fluctuation correspond to the growing part of the instantaneous fluctuation and vice versa. It has been argued earlier, that very close to the jet boundary, the dominant pressure fluctuations are due to the hydrodynamic field which should propagate downstream. Figures 11(a) and (c) show that the carrier wave, underlying the standing wave, propagates downstream.

An additional conspicuous aspect is the quick growth and decay of the organized pressure fluctuation. The hydrodynamic pressure fluctuations are found to grow quickly within a short distance between the nozzle exit and the second shock cell. Subsequently, their amplitude modulates periodically while passing through the periodic shock train. The general decay of the coherent pressure fluctuations occurs after the 4th or 5th shock. This was also visible in the schlieren photographs of Fig. 3. In contrast the organized structures in a fully expanded jet are known to grow at a slower rate over a longer distance, and decay at the end of the potential core.[29]

D. Properties of organized structures

There are two properties of the organized structures discussed in the following: convective velocity and coherent velocity fluctuations. The convective velocity of the organized structures, and the hydrodynamic field created by such structures, were measured by two separate techniques. Both techniques involve measurement of the relative phase variation, $\phi(x)$, with respect to a trigger signal from a fixed microphone and calculating the spatial derivative, $d\phi(x)/dx$, at each measurement station. The convective velocity $u_c$, is normalized by the ambient sound speed c, and is expressed as a convective Mach number:

$$M_c = \frac{u_c}{c} = \frac{2\pi f_s}{\left(c\frac{d\phi}{dx}\right)}.$$

The derivative is calculated from the measured phase variation using a compact three point scheme.[30]

Convective velocity of organized structures

The passage of the organized structures in the jet shear layer was detected by light scattering from a narrow laser beam passing perpendicular to the jet flow direction. The scattered light was sensed by a PMT as shown earlier in Fig. 2. The relative phase ($\phi$) between the PMT signal and that of a fixed microphone was determined by measuring the cross-spectral phase at the screech frequency. The calculations were performed directly through a frequency analyzer (Spectral Dynamics) that provided an average phase over 128 K data points obtained over 6.4 sec. As the laser beam was moved from point to point the relative phase also changed, indicating a convection process. Figures 12(a) and (c) show the measured phase variation in the $M_j = 1.42$ and 1.19 jets along r/D = 0.48. Note that data points are omitted at axial stations where the laser

beam interacts with a shock. Since, a strong scattering by the shock waves completely overwhelms relatively weaker scattering by the organized structures, no phase measurements were possible at these stations.

A careful examination of the phase variation data of Figs. 12(a) and (c) shows an underlying sinuous modulation superimposed on the general linear increase. Such a phase variation is indicative of a non-uniform convective speed which is plotted in Figs. 12(b) and (d) for respectively, $M_j$ = 1.42 and 1.19 jets. The average convective Mach number was also calculated from a least square straight line fit and is found to be 0.68 for the $M_j$ = 1.42 jet and 0.7 for the $M_j$ = 1.19 jet. An examination of the phase variation data of Hu and McLaughlin[22] and Raman and Rice[28] also reveals the same sinuous increase as demonstrated in this paper. The associated phase speed variation, however, remained unnoticed.

There is a relatively large error in the convective velocity calculation, particularly in the region where it is high supersonic. The problem lies with the derivative ($d\phi/dx$) calculation, which amplifies the random error in phase measurement. By repeating measurements at a fixed location, it was determined that the random error introduces a ±2.5° uncertainty in phase data. While this number is very small with respect to the absolute phase value, it becomes significant when difference in phase between two adjacent stations is calculated. When convective speed is high, the difference in phase between two adjacent stations is small, and error in the convective speed calculation is high. The reverse is true when phase speed is low. For example, the true convective Mach number ($M_c$) may be between 3.2-1.5 when the measured value is 2, and it can be between 0.57-0.47 when the measured value is 0.5.

In spite of the measurement error, the large, periodic variation in the phase speed of the organized structures is amply clear in Figs. 12(b) and (d). There are two interesting features which should be pointed out here. First, the convective speed of the organized structures is found to become supersonic ($M_c$ >1) with respect to the ambient sound speed at periodic locations along the jet boundary. According to the "wavy wall analogy[1,29]," the pressure perturbations from such locations should propagate to the farfield. That is, the periodic, spatial, locations where the organized structures reach supersonic convective Mach number are expected to be the effective sound sources. Second, the spatial periodicity ($L_M$) of convective Mach number variation is found to be equal to the standing wave spacing (*not* the shock spacing), $L_M = L_{sw}$. From figures 12(b) and (d), the periodicity of convective Mach number variation is determined to be 0.68D and 1.07D for respectively, $M_j$ = 1.19 and 1.42 jets. A comparison with the various length scales provided in Table I shows that, within the experimental accuracy, the above spatial periodicity is equal to the standing wave spacing. This result has a far-reaching implication, as it shows that the standing wave not only exists outside the jet boundary but inside the jet flow also. In order to verify this conclusion a search was made in the existing literature and the following is a discussion of the outcome.

Turbulent fluctuation in shear layer

In the present program no attempt was made to measure turbulent fluctuations. However, such data are available from prior experiments on underexpanded, screeching jets by Hu and McLaughlin[22] and Raman and Rice.[28] Hu and McLaughlin artificially excited their low Reynolds number, underexpanded jet and performed phase averaged measurements of mass-velocity fluctuation in the shear layer. Raman and Rice measured the axial component of velocity fluctuation in a high Reynolds number jet. In either experiment, the turbulence fluctuation was found to be modulated periodically. The spatial periodicity of the modulation ($L_u$,) is calculated from their data, and is presented in Table II. From the measured data of screech frequency, and the average convective velocity, the expected standing wave spacing ($L_{sw}$) is also calculated. Within the experimental accuracy, the periodicity with which turbulent fluctuations are modulated is found to be the same as that of the standing wave spacing.

Since, the standing wave spacing is found to be the characteristic length scale for the modulation of the organized structures, a cause-and-effect question arises. Does the modulation of organized structure lead to sound generation, or does the nearfield standing wave formation affect the organized structures? This is an important question, as the correct explanation of the unsteady data presented in the earlier section is pivoted on the answer. A further discussion is postponed to the summary and conclusion section.

Convective speed of pressure fluctuations outside jet boundary

The convective speed of the pressure field just outside the jet boundary is expected to be similar to that of its primary originators, the large organized structures. The measurement technique, however, is completely different as the flow velocity is very small and a microphone can be placed to measure pressure fluctuation. An additional difference is the measurement locations. The laser light scattering technique was used inside the shear layer, at r/D = 0.48, and the traverses were made parallel to the jet centerline. The microphone traverses were made outside the shear layer, and along the oblique line for which amplitude modulation of pressure fluctuation is reported (Fig. 11). Like before, the microphone was closest to the

jet at the nozzle lip (r/D= 0.6 and 0.7 for respectively $M_j$ = 1.19 and 1.42 jets) and was traversed at an angle of 5.71° to the jet axis. The relative phase ($\phi$) between the traversing and a fixed microphone was measured from the cross-spectral phase at the screech frequency. The phase and convective Mach number variation data are presented in figures 13 for both $M_j$ = 1.19 and 1.42 jets. In addition, the root-mean-square of the fluctuating pressure ($p_{rms}$)at the screech frequency is also plotted (Figs. 13(c) and (f)).

The microphone measurement has the advantage of providing data points even over the axial locations where shocks are present in the shear layer. The discontinuities in Fig. 12 are absent in Fig. 13. Nevertheless, the critical features are common. The convective speed is found to vary from a supersonic to subsonic value with a periodicity identical to that of the standing wave spacing. Noticeably, a minima in the standing wave amplitude (Figs. 13(c) and (f)) corresponds to a minima in the convective velocity and vice versa.

## V. Summary and Conclusion

An experimental investigation of the intricate dynamics that lead to screech noise generation and propagation is presented in this paper. The detailed, unsteady experimental data are of primary value. A preliminary analysis of the experimental data is found to produce some new observations. Following is a summary, and a discussion of various issues at hand.

The pressure fluctuations in the nearfield region of the jets are found to be composed of two components: acoustic and hydrodynamic. The latter is due to the potential field of the turbulent fluctuations present in the jet shear layer. Spark schlieren photographs of the screeching jets show that the major part of the turbulent fluctuations is due to large, periodic coherent vortices that propagate with the flow. The nearfield, root-mean-square pressure fluctuation data, at the screech frequency, show the presence of two interconnected standing wave patterns. The first one is along the jet boundary, and the second one is along a diagonal line that marks the boundary of forward propagation of the fundamental frequency. It is demonstrated that both of the patterns are the outcome of a standing wave formation between the hydrodynamic and acoustic pressure fluctuations.

It is also shown that an exact expression of the screech frequency can be obtained from the standing wave relationship mentioned above. In the past, Powell[5,14] has obtained a similar expression for screech frequency based on the feedback loop consideration. Fisher and Morfey[16] and Tam *et al.*[17] came up with two separate expressions by relating screech as a special case of broadband shock associated noise. It is demonstrated that all of the above relations can be obtained from the standing wave relation with suitable approximations.

Interestingly, the standing wave formation is found to permeate into the jet and affect the organized turbulent structures in the shear layer. This was observed from a measurement of the convective velocity of such structures. The convective velocity is found to gyrate periodically from low subsonic to moderately supersonic with respect to the ambient sound speed. The spatial periodicity is found to be the same as that of the standing wave. Some additional support is obtained from the turbulent fluctuation measurement of Hu and McLaughlin[22] and Raman and Rice.[28] An analysis of their data show that the periodic growth and decay of shear layer turbulent fluctuations occur with the same periodicity as that of the standing waves expected in their facilities.

The above observation brings up an important cause-and-effect question. Are the periodic modulations of organized turbulence the effect of the standing wave formed outside the jet, or is the outside pressure field a consequence of the modulations already present inside the jet? The former implies that the acoustic fluctuations outside the jet boundary strongly influence turbulence fluctuations inside the jet. The latter implies the presence of an inherent length scale (that of the standing wave spacing), which selects the frequency at which screech sound will be generated by the jet. The natural selection is such that the resultant of acoustic and hydrodynamic wavelengths satisfies the standing wave scale already present inside the jet. No definite answer can be provided at this time; however, the first possibility is somewhat dubious and the second possibility cannot be ruled out. It is known that a fully developed turbulent shear layer is poorly receptive to acoustic disturbances. The shear layer over the third, fourth and subsequent shock cells is fully developed, and is not expected to be influenced by an independently formed standing wave outside the flow boundary. On the other hand, Tables I and II show that the standing wave spacing, albeit different, is closely related to the average shock spacing. The fundamental fourier mode of pressure perturbation, in the sense of shock formation analysis by Tam *et al*,[31] may coincide with the standing wave spacing.

It has already been mentioned that the convective velocity and coherent fluctuations are modulated periodically with the standing wave spacing. This observation provides a curious confluence of the various sound generation processes proposed so far. According to the wavy wall analogy of sound generation[1,29] the pressure

field associated with a passing organized structure is radiated in the far field whenever the organized structure reaches a supersonic speed relative to the ambient media. Clearly, for the present screeching jets, acoustic radiation should occur from multiple sources, placed a standing wavelength distance apart, where the organized structures reach supersonic speed. Interestingly, a distinction has to be made between the 'Mach wave' radiation process described by Tam[1] and Morris[29] and the screech generation process outlined above. In 'Mach wave' radiation, the convective Mach number of the turbulent vortices remain supersonic over a considerable distance, while, for the present screech process, supersonic convective velocity is attained periodically at only a few selective locations along the jet boundary. The sound sources are, therefore in a sense, spatially stationary as opposed to convecting. A second, parallel argument for the screech source is provided by Hu and McLaughlin.[22] Using Liu's[32] postulate of the decay of coherent fluctuation as the source of noise production, they proposed that the periodic locations where coherent fluctuations decay are the noise sources. It is shown in Table II of this paper, that the periodic dips in turbulent fluctuations are at the standing wave spacing. Therefore, once again, multiple sound sources that are a standing wavelength distance apart are expected to be present in a screeching jet. The phase variation measurements of Figs. 13(a) and (d) show that there exists a nearly constant phase difference in the pressure fluctuations measured between the source locations. This is in agreement with Powell's screech directivity model, where multiple sound sources were assumed to be radiating sound with a constant phase difference.

Returning back to the cause-and-effect question, there is now sufficient evidence to believe that the periodic peaks and valleys in the root-mean-square pressure fluctuation data of Fig. 5 are the consequence of periodic sources, placed a standing wavelength apart, inside the jet. The unsteady, phase averaged, nearfield pressure fluctuation data of Figs. 8 to 11 can also be reinterpreted. Note that only a small part of the visual gala, obtained from color plots of the measured data, can be presented in this paper. A video animation of the interaction process has been made, which clarifies that the sound waves are created from a periodic modulation of the hydrodynamic pressure waves lying just outside the jet boundary. The source of the compression or the rarefaction part of the sound is a similar fluctuation of the hydrodynamic wave lying between the third and the fourth shock from the nozzle exit. The sound wave gains further strength as it propagates primarily in the upstream direction over the multiple, periodically placed sources. The sound directivity pattern is governed by the multiple, phased-array, source model of Powell. By following an upstream propagating acoustic wave it is found that the motion has a curious pause-and-go feature. The compression or rarefaction part of the acoustic fluctuation gains strength as it pauses over a similar hydrodynamic fluctuation. The harmonics of the screech frequency are also believed to be generated from sources located inside the jet.

## Acknowledgment

The author acknowledges help in setting up the schlieren system, from Ken E. Weiland and Carolyn R. Mercer of NASA Lewis.

## Reference

1. Tam, C.K.W., "Jet Noise Generated by Large-Scale Coherent Motion," *Aeroacoustics of Flight Vehicles: Theory and Practice*, vol. 1: Noise Sources, NASA RP-1258, WRDC TR-90-3052, H. H. Hubbard, ed., 1991, pp. 311–390.
2. Seiner, J.M., Manning, J.C. and Ponton, M.K., "Model and Full Scale Study of Twin Supersonic Plume Resonance," AIAA–87–0244, Jan. 1987.
3. Hay, J.A. and Rose, E.G., "In Flight Shock Cell Noise," *J. Sound & Vib.*, vol. 11, 1970, pp. 411–420.
4. Cain, A.B., Bower, W.W., Walker, S.H. and Lockwood, M.K., "Modeling Supersonic Jet Screech Part 1: Vortical Instability Wave Modeling," AIAA Paper No. 95–0506, presented at 33rd Aerospace Sciences Meeting, 1995.
5. Powell, A., "On The Mechanism of Choked Jet Noise," *Proc. phys. Soc. (London)*, Vol. 66, pt. 12, 1953, No. 408B, pp. 1039–1056.
6. Yu, J.C. and Seiner, J.M., "Nearfield Observations of Tones Generated from Supersonic Jet Flows," AIAA Paper No. 83–0706, 1983.
7. Seiner, J.M., "Advances in High Speed Jet Acoustics," AIAA Paper No. 84–2275, Oct. 1984.
8. Poldervaart, L.J., Vink, A.T. and Wijnands, A.P.J., "The photographic evidence of the feedback loop of a two dimensional screeching supersonic jet of air," presented at the 6th International Congress on Acoustics, Tokyo, Japan, August 21-28, 1968.
9. Rice, E.J. and Taghavi, R., "Screech Noise Source Structures of a Supersonic Rectangular Jet," AIAA Paper No. 92–0503, 30th Aerospace Sciences Meeting & Exhibit, 1992.
10. Norum, T.D. and Seiner, J.M., "Location and Propagation of Shock Associated Noise from Supersonic Jets," AIAA Paper No. 80–0983, 1980.
11. Westley R., and Woolley, J.H., "An Investigation of the Near Noise Fields of a Choked Axisymmetric Air Jet," *Aerodynamic Noise*, University of Toronto Press, 1968, pp. 147–167.

12. Westley R., and Woolley, J.H., "The Near Field Sound Pressures of a Choked Jet During a Screech Cycle," Aircraft Engine Noise and Sonic Boom, AGARD CP-42, AGARD, Neuilly-Sur-Sein, France, 1969, Paper 23.
13. Westley R., and Woolley, J.H., "Shock Cell Noise-Mechanisms, The Near Field Sound Pressure Associated With a Spinning Screech Mode," Presented at the Conference on Current Developments in Sonic Fatigue, Institute of Sound and Vibration Research, University of Southampton, July 1970.
14. Powell, A., "On the Noise Emanating from a Two-Dimensional Jet Above the Critical Pressure," *The Aeronautical Quarterly*, Vol. IV, 1953, pp. 103–122.
15. Norum, T.D., "Screech Suppression in Supersonic Jets," *AIAA J.*, Vol. 21, No. 2, pp. 235–240, Feb. 1983.
16. Fisher, M.J., and Morfey, C.L., "Jet Noise," in *AGARD Lecture Series No. 80, Aerodynamic Noise,* Dec. 1976.
17. Tam, C.K.W., Seiner, J.M. and Yu, J.C., "Proposed Relationship Between Broadband Shock Associated Noise and Screech Tones," *J. Sound & Vib.*, Vol. 110 (2), 1986, pp. 309–321.
18. Morris, P.J., Bhat, T.S.R. and Chen, G., "A Linear Shock Cell Model For Jets of Arbitrary Exit Geometry," *J. Sound Vib.*, Vol. 132, No. 2, pp. 199–211, 1989.
19. Panda, J., "Measurement of Shock Oscillation in Underexpanded Supersonic Jets," AIAA Paper No. 95–2145, 26th AIAA Fluid Dynamics Conference, San Diego, CA, June 1995.
20. Panda, J., "A Shock Detection Technique Based on Light Scattering by Shock," *AIAA J.*, Vol. 33, No. 12, pp. 2431–2433, Dec. 1995.
21. Davis, M.G. and Oldfield, D.E.S., "Tones From a Chocked Axisymmetric Jet. I. Cell Structure, Eddy Velocity and Source Locations," *Acustica*, Vol. 12, No. 4, pp. 257–277, 1962.
22. Hu, T.F. and McLaughlin, D.K., "Flow and acoustic properties of low mach number underexpanded supersonic jets," *J. Sound Vib.*, Vol. 141, pp. 485, 1990.
23. Truman, C.R., "The Influence of Turbulent Structures on Optical Phase Distortion Through Turbulent Shear Flows," AIAA Technology Conf., 1992.
24. Strohben, J.W., ed., "Laser Beam Propagation in the Atmosphere," Springer-Verlag, 1978.
25. Dahl, M.D., "The Aeroacoustics of Supersonic Coaxial Jets," Ph. D. dissertation, The Pennsylvania State University, 1994. Also NASA TM–106782.
26. Pack, D.C., "A Note on Prandtl's Formula for the Wavelength of a Supersonic Gas Jet," *Quart. Journ. Mech. and Applied Math.*, Vol. 111, Pt. 2, 1950.
27. Walker, W.H., Gordeyev, S.V. and Thomas, F.O., "A Wavelet Analysis Applied to Unsteady Jet Screech Resonance," ASME Fluids Engineering Conf., Forum on High Speed Jets, Aug. 1995.
28. Raman, G. and Rice, E.J., "Instability modes excited by natural screech tones in a supersonic rectangular jet," *Physics of Fluids*, Vol. 6, No. 2, pp. 3999–4008, Dec. 1994.
29. Morris, P.J., "Flow Characteristics of the Large Scale Wave Like Structure of a Supersonic Round Jet," *J. Sound & Vib.*, Vol. 53, No. 2, 1977, pp. 223–244.
30. Anderson, Tennehill and Pletcher, "Computational Fluid Dynamics,"
31. Tam, C.K.W. and Jackson, J.A., "A Multiple-scales Model of the Shock-cell Structures of Imperfectly Expanded Supersonic Jets," *J. Fluid Mech.*, Vol. 153, pp. 123–149, 1985.
32. Liu, J.T.C., "Developing large-scale wavelike eddies and the near jet noise field," *J. Fluid Mech.*, Vol. 62, 1974, pp. 437–464.

TABLE I.—LENGTH SCALES RELEVANT TO THE NEARFIELD PATTERN ALONG JET BOUNDARY

| $M_j$ | Average spacing between pressure crests ($L_p/D$) | Wavelength, acoustic ($\lambda_s/D$) | Wavelength, hydrodynamic ($\lambda_h/D$) | $\left(\frac{D}{\lambda_s}+\frac{D}{\lambda_h}\right)^{-1}$ | Average shock spacing (L/D) |
|---|---|---|---|---|---|
| 1.19 | 0.67 | 1.59 | 1.15 | 0.66 | 0.77 |
| 1.42 | 1.02 | 2.49 | 1.74 | 1.03 | 1.28 |

TABLE II.—LENGTH SCALES RELEVANT TO THE MODULATION OF TURBULENT FLUCTUATIONS (u') IN JET SHEAR LAYER

| $M_j$ | Screech frequency $f_s$, Hz | Convective Mach number ($M_c$) | Expected standing wave spacing[a] ($L_{sw}/h$) | Average shock of u' modulation ($L_u/h$) | Average shock spacing (L/h) |
|---|---|---|---|---|---|
| [b]2.44 | 7936 | 0.78 | 2.61 | 2.57 | 2.0 |
| [c]1.55 | 6336 | 0.78 | 3.24 | 3.17 | 2.5 |
| [d]2.1 | 9442 | 1.02 | 1.9 | 2.0 | 1.34 |

[a]Normalizing parameter h represents the small nozzle dimension for rectangular jet, and diameter for circular jet.

[b]Reference 28; rectangular jet.

[c]G. Raman, personal communication; rectangular jet.

[d]Reference 22, circular jet.

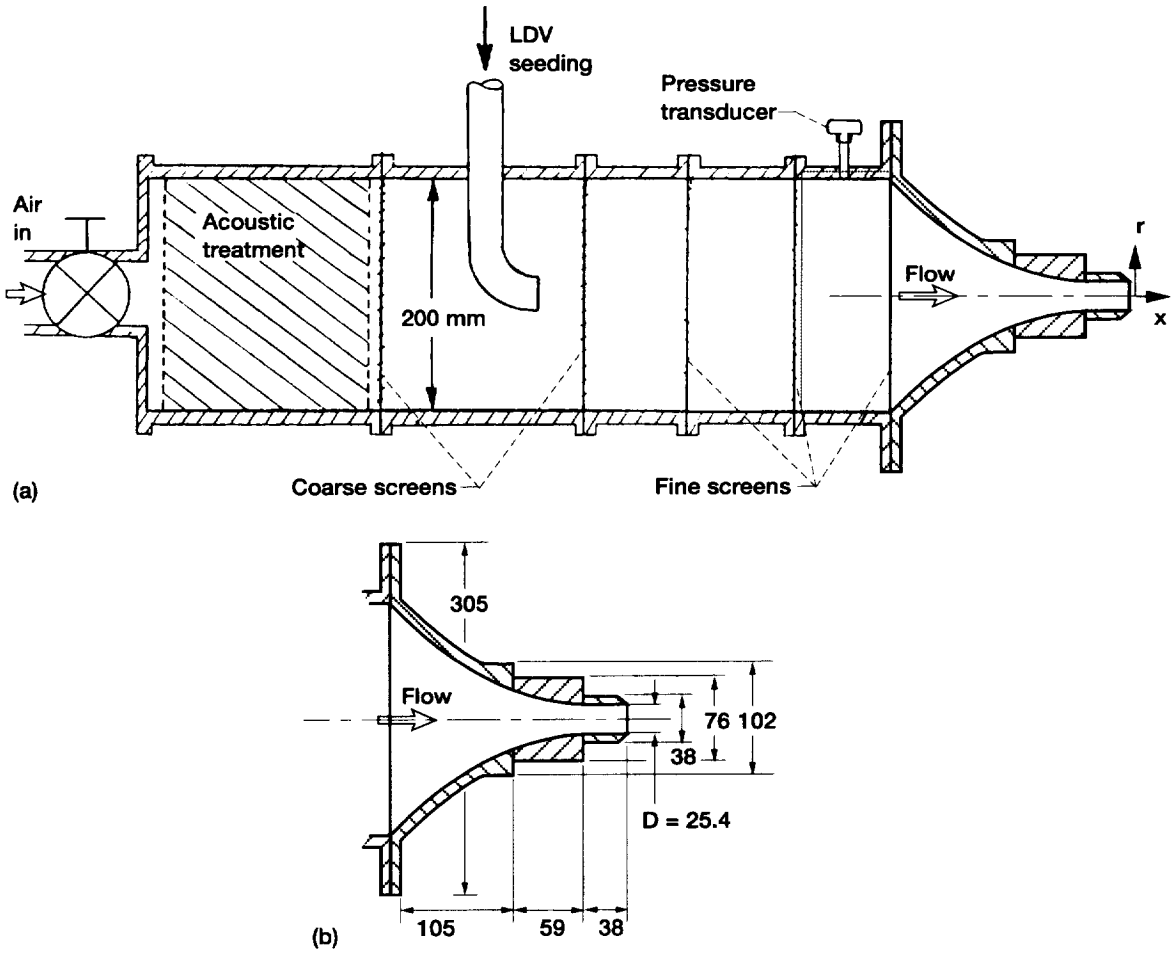


Figure 1.—The jet facility. (a) Schematic. (b) Detail of the nozzle block, all dimensions are in millimeter.

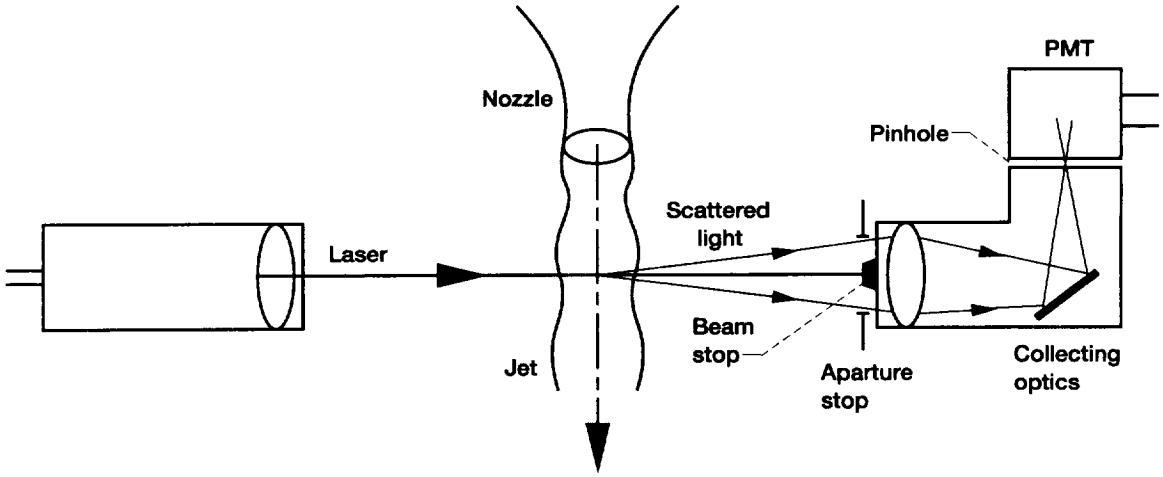


Figure 2.—A schematic of the optical arrangement to detect laser light scattered by the jet flow.

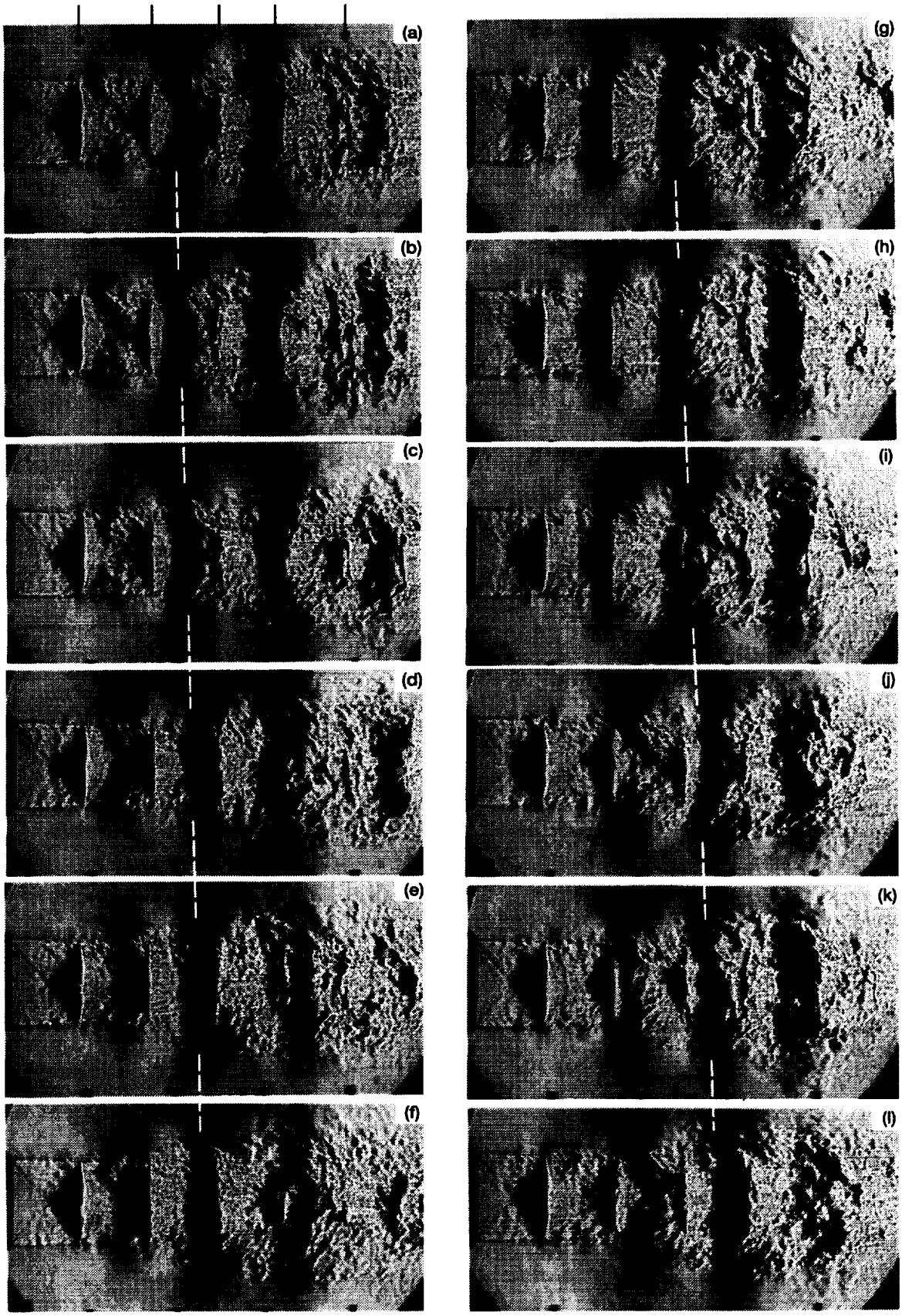


Figure 3.—Spark schlieren visualization of $M_j = 1.19$ jet at 12 equispaced phases over a screech cycle. Vertical arrows in photograph (a) indicate shocks. The chain line joins positions of one organized structure.

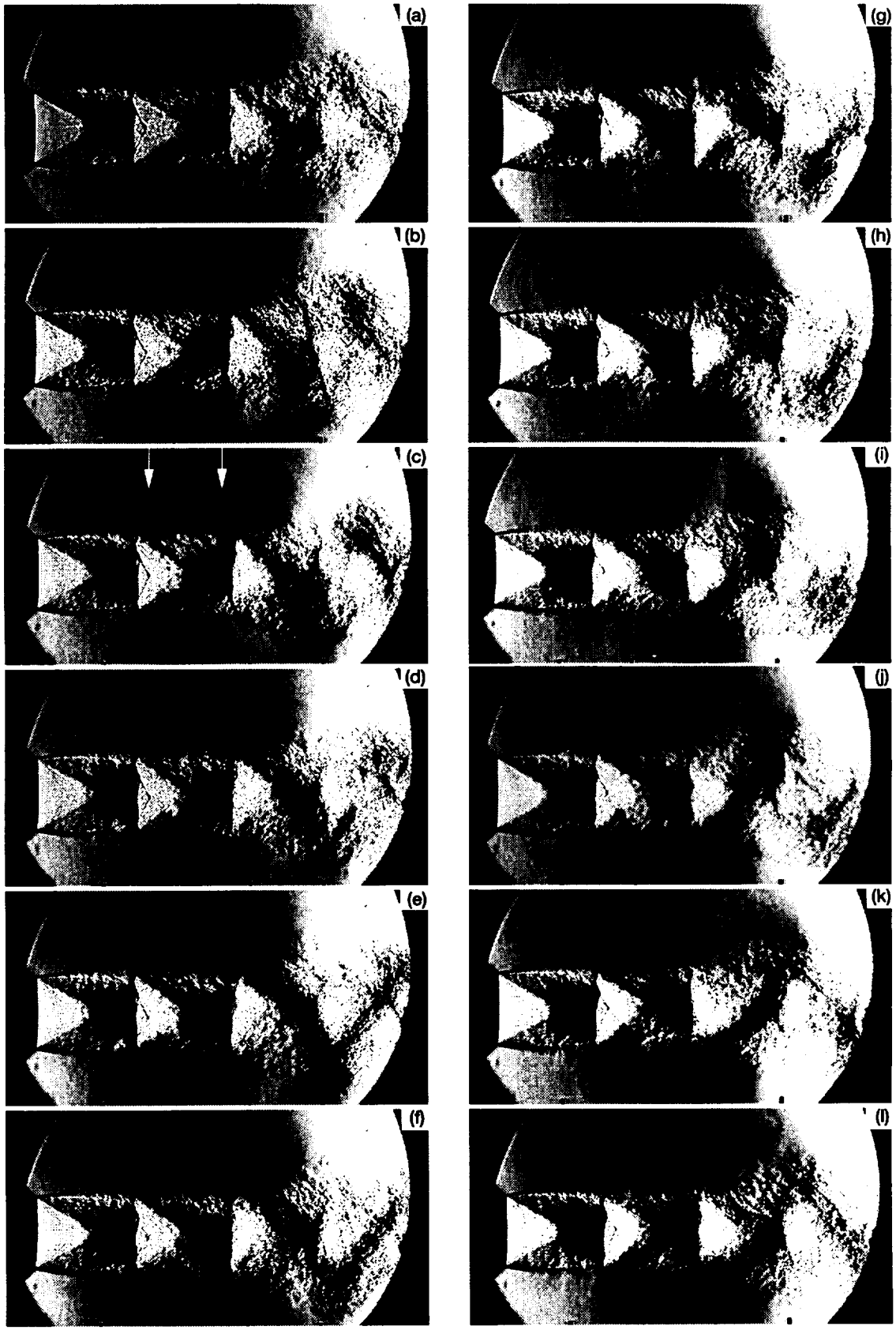


Figure 4.—Phase averaged schlieren photographs of $M_j = 1.42$ jet at 12 equispaced phases over a screech cycle.

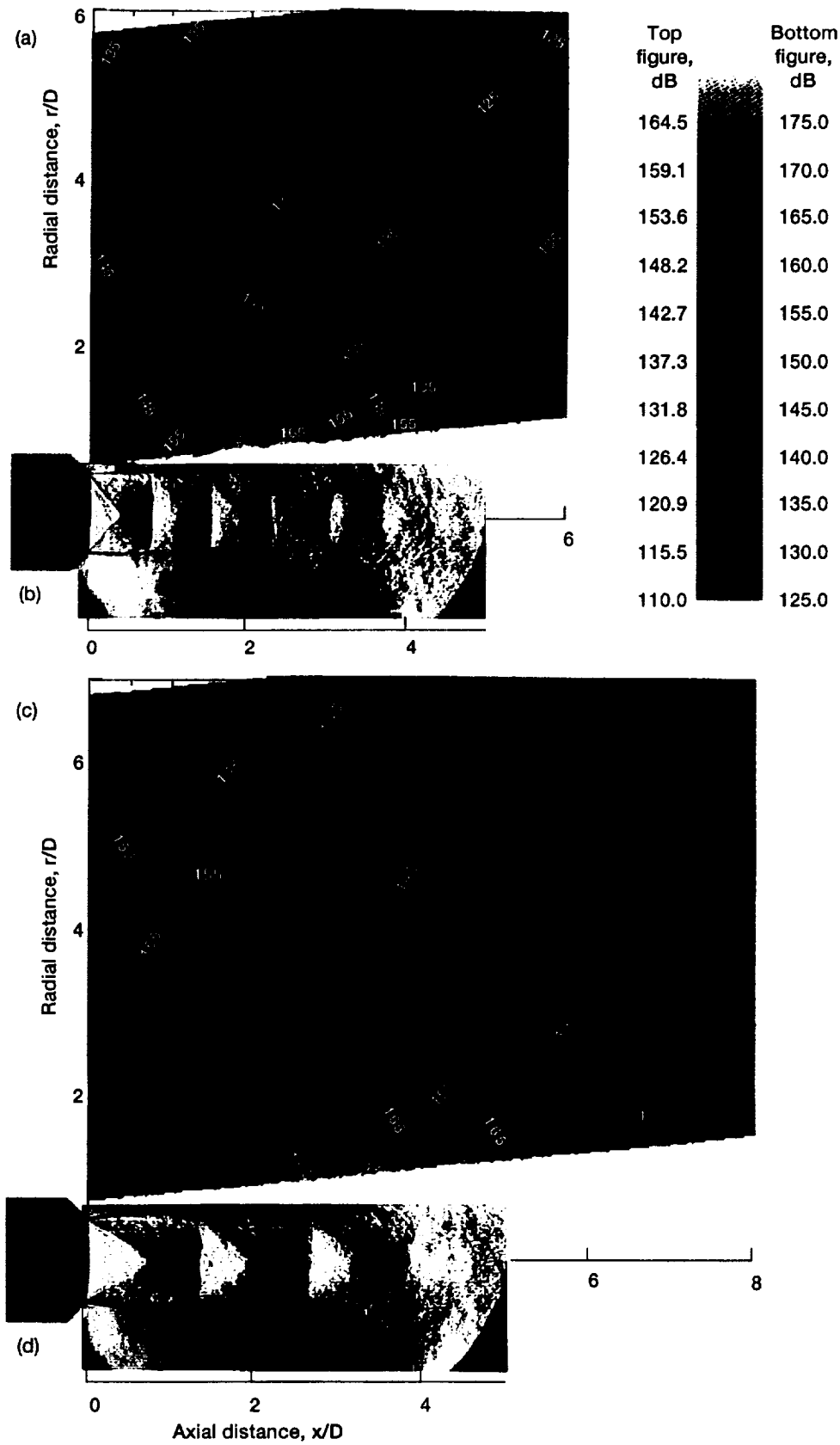


Figure 5.—RMS pressure fluctuations at screech frequency and schlieren photograph for (a), (b) $M_j = 1.19$ and (c), (d) 1.42 jets. The superimposed contour levels are at 5 dB intervals.

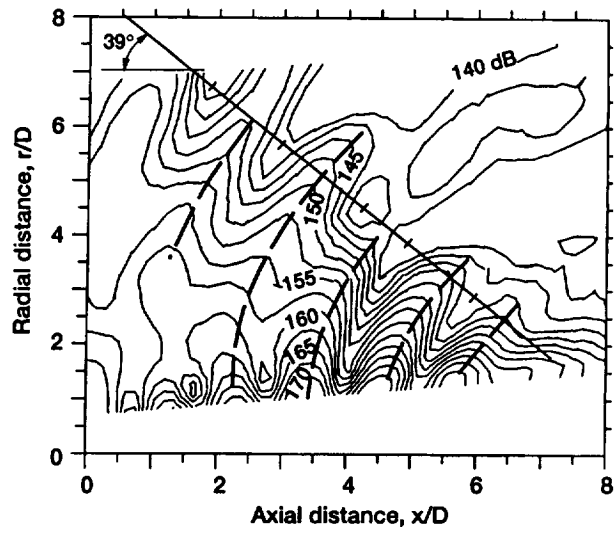


Figure 6.—Same as figure 5(c), except for the absence of color. The contour levels are at 2.5 dB interval. The curved chain line joins the local maxima in the contours; the straight line joins diagonal red-blue pattern of figure 5(c).

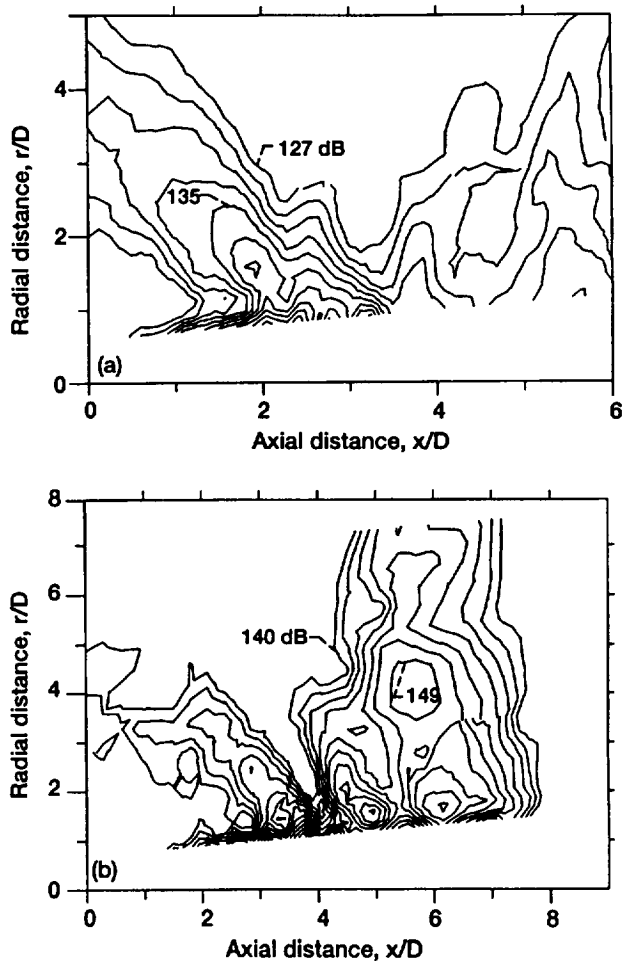


Figure 7.—RMS pressure fluctuation at twice the screech frequency for (a) $M_j$ = 1.19 and (b) 1.42 jets. The contour levels are at (a) 2 dB and (b) 1.5 dB intervals.

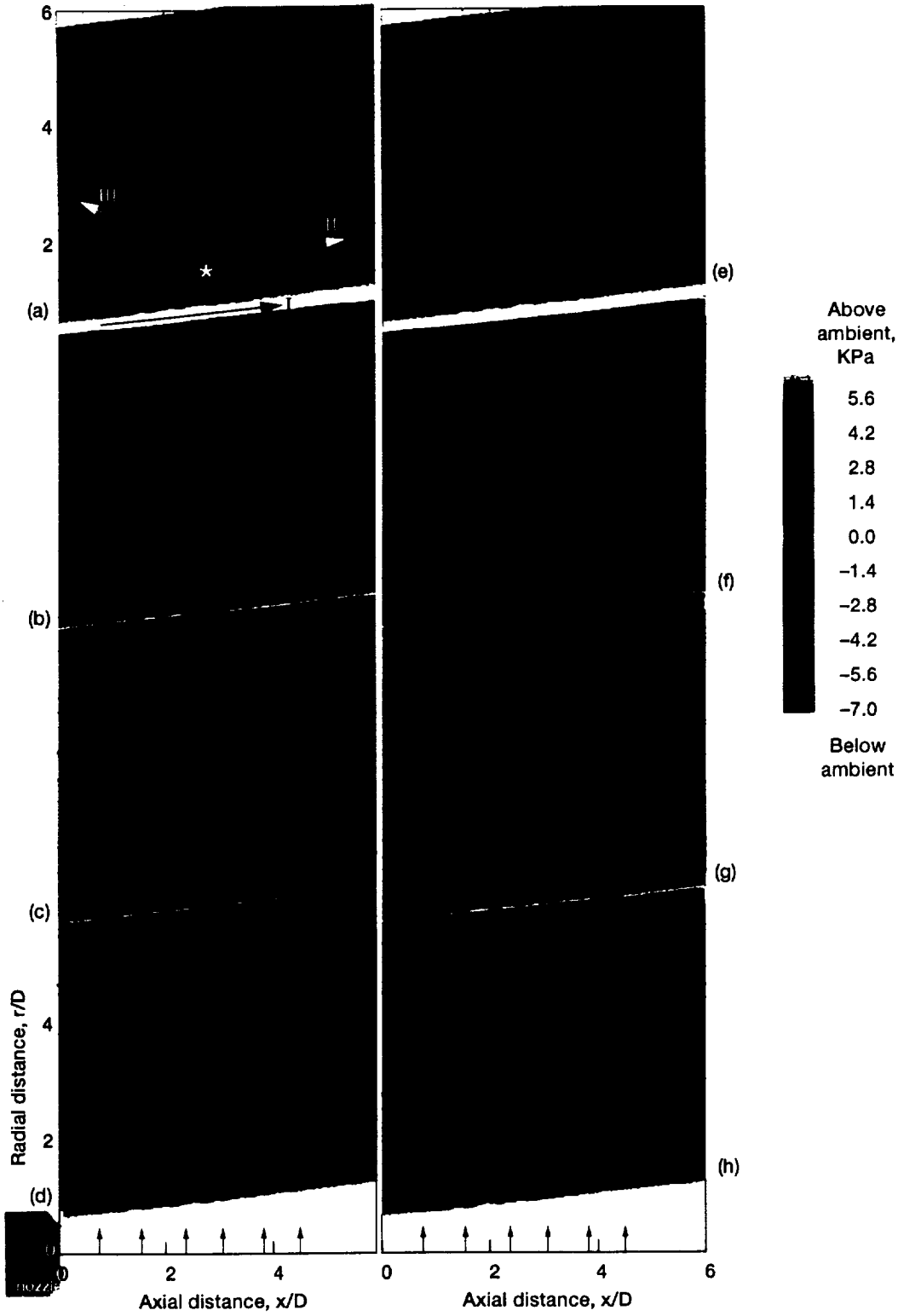


Figure 8.—Phase averaged fluctuating pressures, <p>, for $M_j$ = 1.19 jet. Phase time $\tau/T$ for (a)-(h): 0, 0.125, 0.25, 0.375, 0.50, 0.625, 0.75 and 0.875. The contour levels are at an interval of 150 Pa. Dashed contours represent below ambient and solid ones above ambient pressure. Arrow I shows the motion of hydrodynamic waves, and II & III that of acoustic waves. The vertical arrows at bottom represent shock locations.

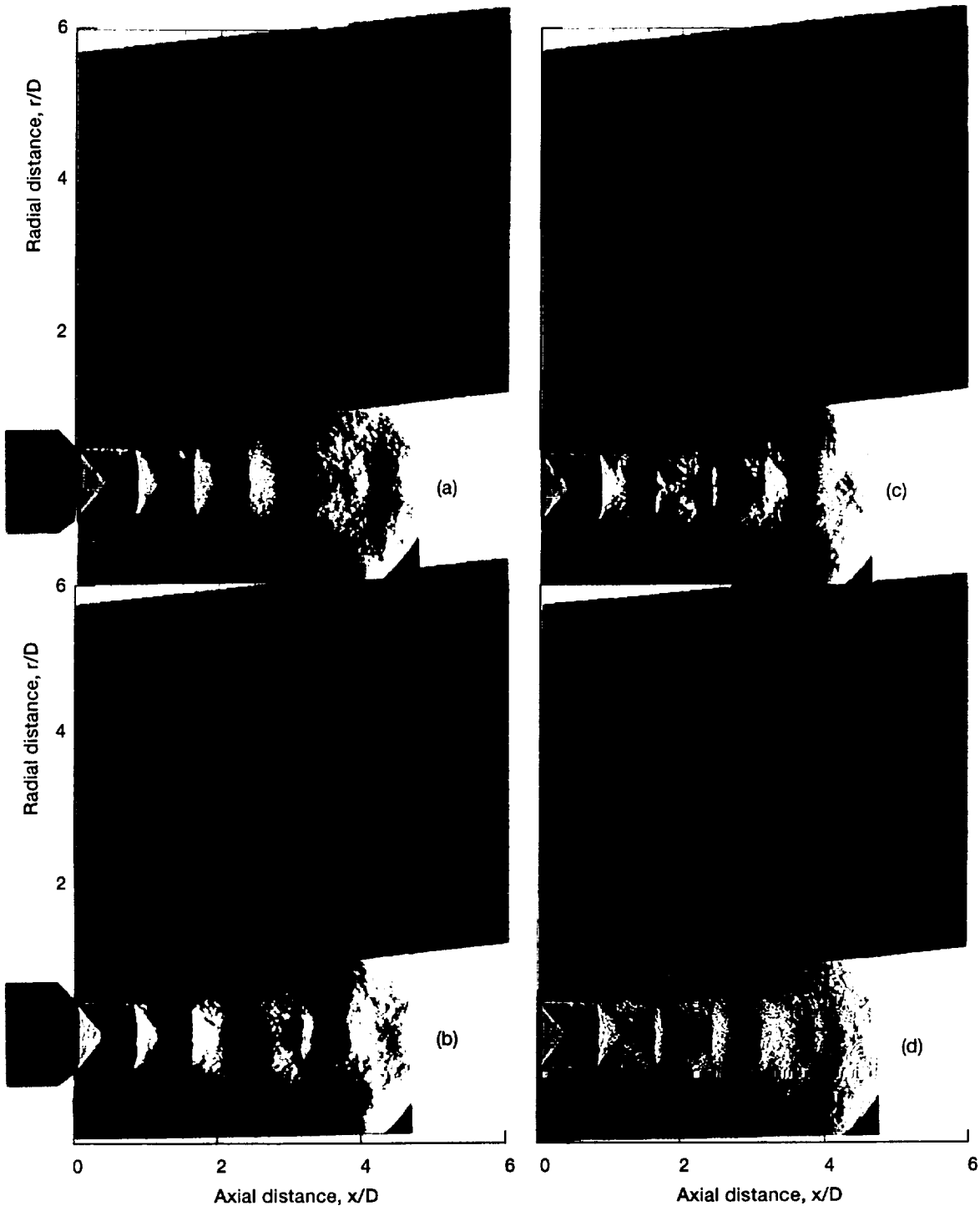


Figure 9.—Phase averaged schlieren photographs and fluctuating pressures, <p>, at 4 different phases; (a) $\tau/T = 0$, (b) = 0.25, (c) = 0.5, (d) = 0.75, of screech cycle in $M_j = 1.19$ jet. The fluctuating pressure data are the same as in figures 8(a), (c), (e), and (g).

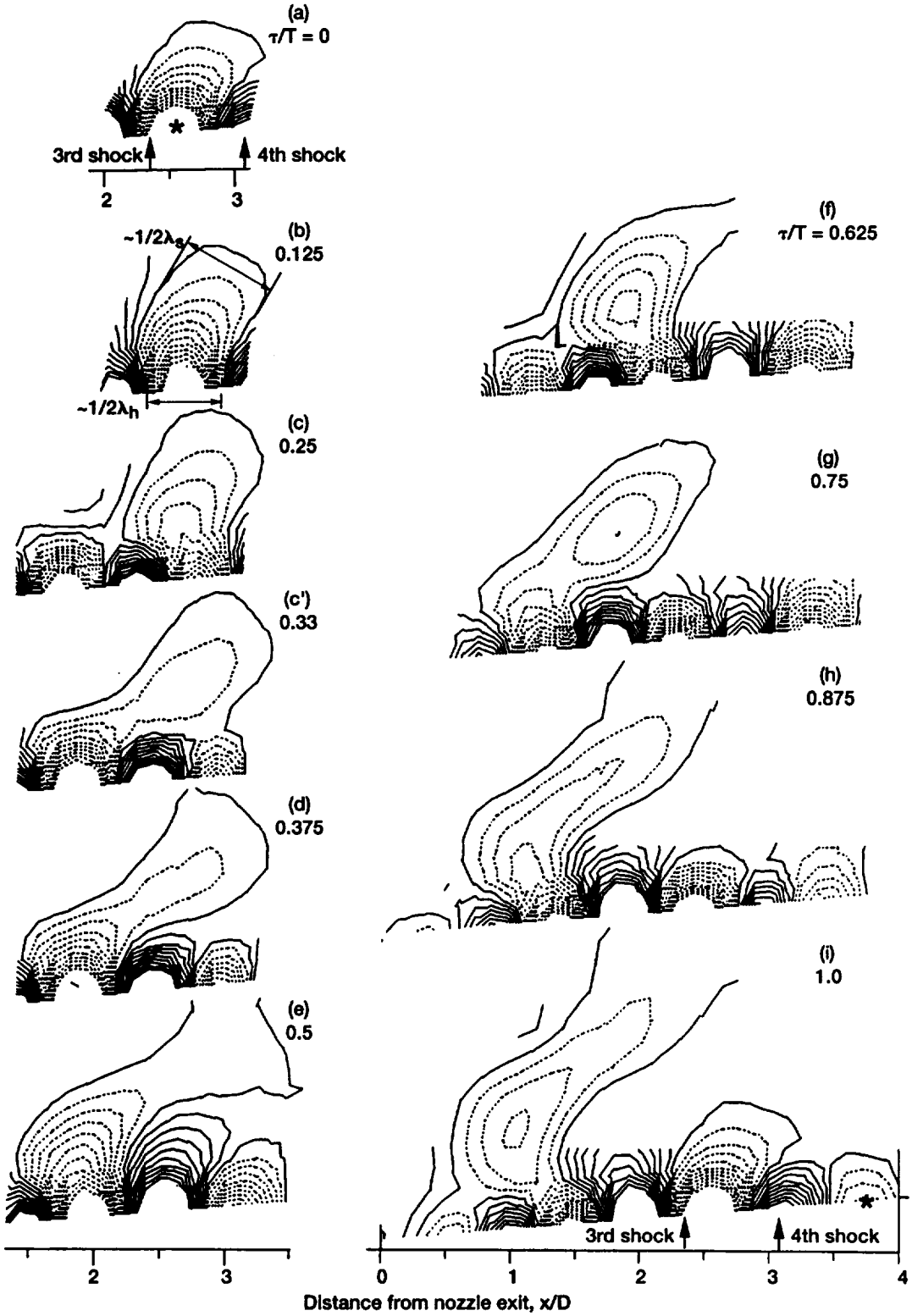


Figure 10.—Selected regions of figure 8 are replotted to highlight the dynamics of one rarefaction region. The contour descriptions are also identical. Phase times τ/T are as indicated.

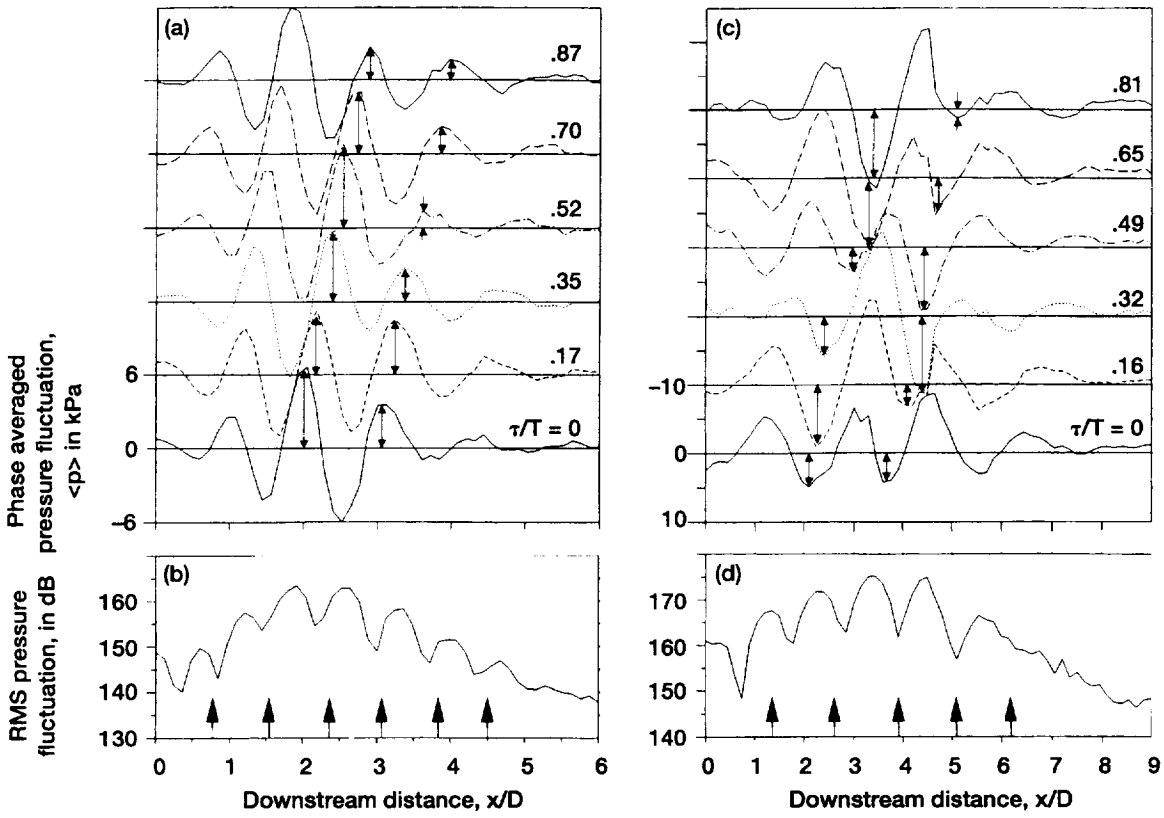


Figure 11.—Phase averaged and rms pressure fluctuations just outside the boundaries of (a), (b) $M_j = 1.19$, and (c), (d) $M_j = 1.42$ jets. Each plot of (a) and (c) is shifted by a major division as shown by horizontal lines. Phase times are as indicated. The double sided arrows show modulation of compression or rarefaction zone, and single sided arrows show shock locations.

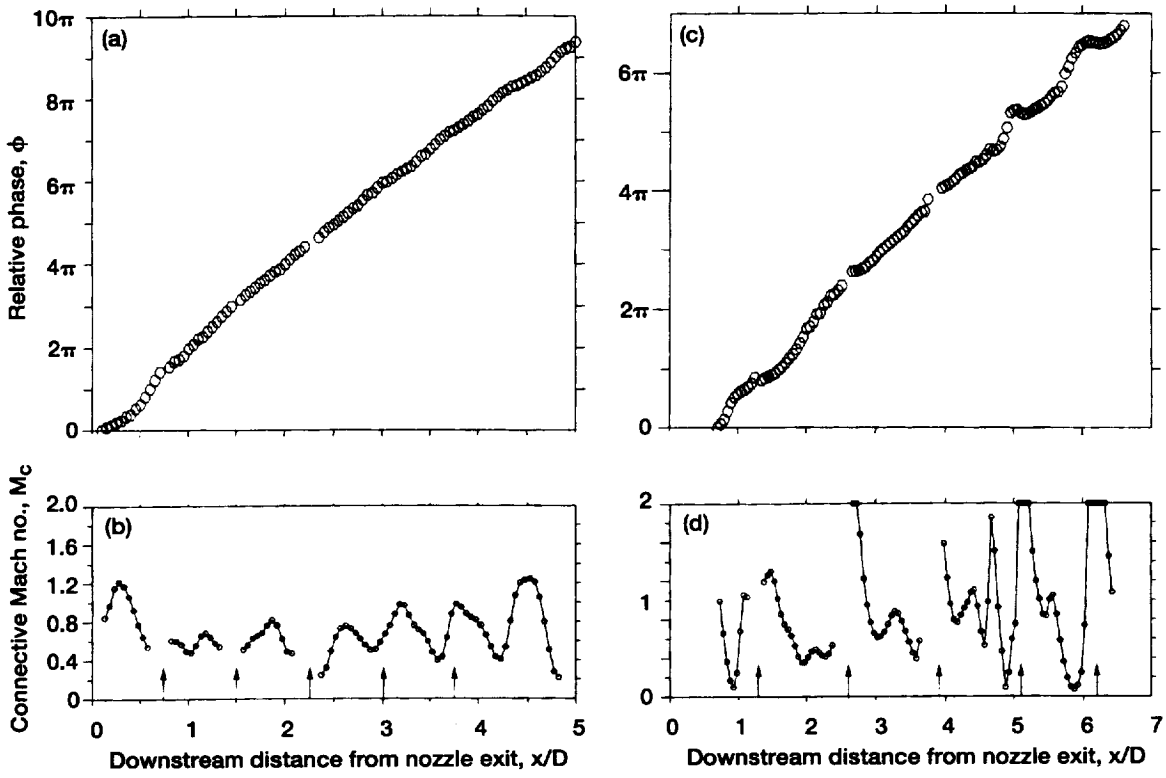


Figure 12.—Phase and convective Mach number variations in (a), (b) $M_j$ = 1.19 and (c), (d) 1.42 jets along r/D = 0.48. Data obtained by laser light scattering from organized structures. The vertical arrows at the bottom of (b) and (d) represent shock locations.

# REPORT DOCUMENTATION PAGE

*Form Approved*
*OMB No. 0704-0188*



| 1. AGENCY USE ONLY (*Leave blank*) | 2. REPORT DATE | 3. REPORT TYPE AND DATES COVERED |
|---|---|---|
| | April 1996 | Final Contractor Report |

**4. TITLE AND SUBTITLE**

An Experimental Investigation of Screech Noise Generation

**5. FUNDING NUMBERS**

WU–505–62–53
C–NAS3–27377

**6. AUTHOR(S)**

J. Panda

**7. PERFORMING ORGANIZATION NAME(S) AND ADDRESS(ES)**

Modern Technologies Corporation
7530 Lucerne Drive
Islander Two, Suite 206
Middleburg Heights, Ohio 44130

**8. PERFORMING ORGANIZATION REPORT NUMBER**

E–10096

**9. SPONSORING/MONITORING AGENCY NAME(S) AND ADDRESS(ES)**

National Aeronautics and Space Administration
Lewis Research Center
Cleveland, Ohio 44135–3191

**10. SPONSORING/MONITORING AGENCY REPORT NUMBER**

NASA CR–198467
AIAA–96–1718

**11. SUPPLEMENTARY NOTES**

Prepared for the 2nd Aeroacoustics Conference cosponsored by the American Institute of Aeronautics and Astronautics and the Confederation of European Aerospace Societies, State College, Pennsylvania, May 6–8, 1996. Project Manager, John Abbott, Internal Fluid Mechanics Division, NASA Lewis Research Center, organization code 2660, (216) 433–3607.

**12a. DISTRIBUTION/AVAILABILITY STATEMENT**

Unclassified - Unlimited
Subject Categories 71, 34 and 7

This publication is available from the NASA Center for AeroSpace Information, (301) 621–0390.

**12b. DISTRIBUTION CODE**

**13. ABSTRACT** ***(Maximum 200 words)***

The screech noise generation process from supersonic underexpanded jets, issuing from a sonic nozzle at pressure ratios of 2.4 and 3.3 (fully expanded Mach number, $M_j$ = 1.19 and 1.42), was investigated experimentally. Spark schlieren visualization at different phases of the screech cycle clearly shows the convection of the organized turbulent structures, and the associated hydrodynamic pressure field, over a train of shock waves. The rms pressure fluctuation at the screech frequency was measured in the nearfield region by a traversing microphone. The data show the presence of two sets of interconnected peak and valley patterns: one along the jet boundary and the other along a diagonal direction. Both of these patterns are shown to be an outcome of a standing wave formation between the upstream propagating acoustic and downstream propagating hydrodynamic fluctuations. Laser light scattering by turbulence was utilized to measure convective velocity of the organized structures. The convective velocity is found to change periodically from subsonic to supersonic values with respect to the ambient sound speed. Interestingly, the periodicity is found to be the same as that of the standing wave spacing. For the round jet under consideration, the standing wave spacing is smaller than the shock wave spacing. An analysis of data obtained by Raman and Rice (1994) and Hu and McLaughlin (1990) reveals that the turbulent fluctuations are also modulated periodically at the standing wave spacing expected in their facilities. It is demonstrated that the existing screech frequency formulae can be derived from the simple standing wave relationship between the acoustic and the hydrodynamic fields. Based on the above observations and additional support from the supersonic wavy wall analogy, it is proposed that there exist multiple sound sources, equispaced by a standing wavelength, in the jet shear layer. The time evolution of the pressure fluctuations over the nearfield region was obtained from phase averaged microphone measurements. An analysis of this data further clarifies the sound generation process. The coherent hydrodynamic fluctuations are identifiable within a short distance from the jet boundary. They have a short wavelength, propagate downstream with the flow and, their amplitude is modulated periodically with the standing wave spacing. The relatively weak and longer wavelength acoustic fluctuations are found to originate from the hydrodynamic fluctuations. By following an upstream propagating acoustic wave, it is found that the source of the compression or the rarefaction part is a similar hydrodynamic fluctuation lying approximately between the 3rd and the 4th shock. Subsequently, the acoustic wave propagates in a curious pause-and-go, walking motion over the modulated hydrodynamic field. Such interactions further strengthen the acoustic wave.

| 14. SUBJECT TERMS | 15. NUMBER OF PAGES |
|---|---|
| Aeroacoustics; Supersonic jets; Screech | 27 |
| | 16. PRICE CODE: A03 |

| 17. SECURITY CLASSIFICATION OF REPORT | 18. SECURITY CLASSIFICATION OF THIS PAGE | 19. SECURITY CLASSIFICATION OF ABSTRACT | 20. LIMITATION OF ABSTRACT |
|---|---|---|---|
| Unclassified | Unclassified | Unclassified | |

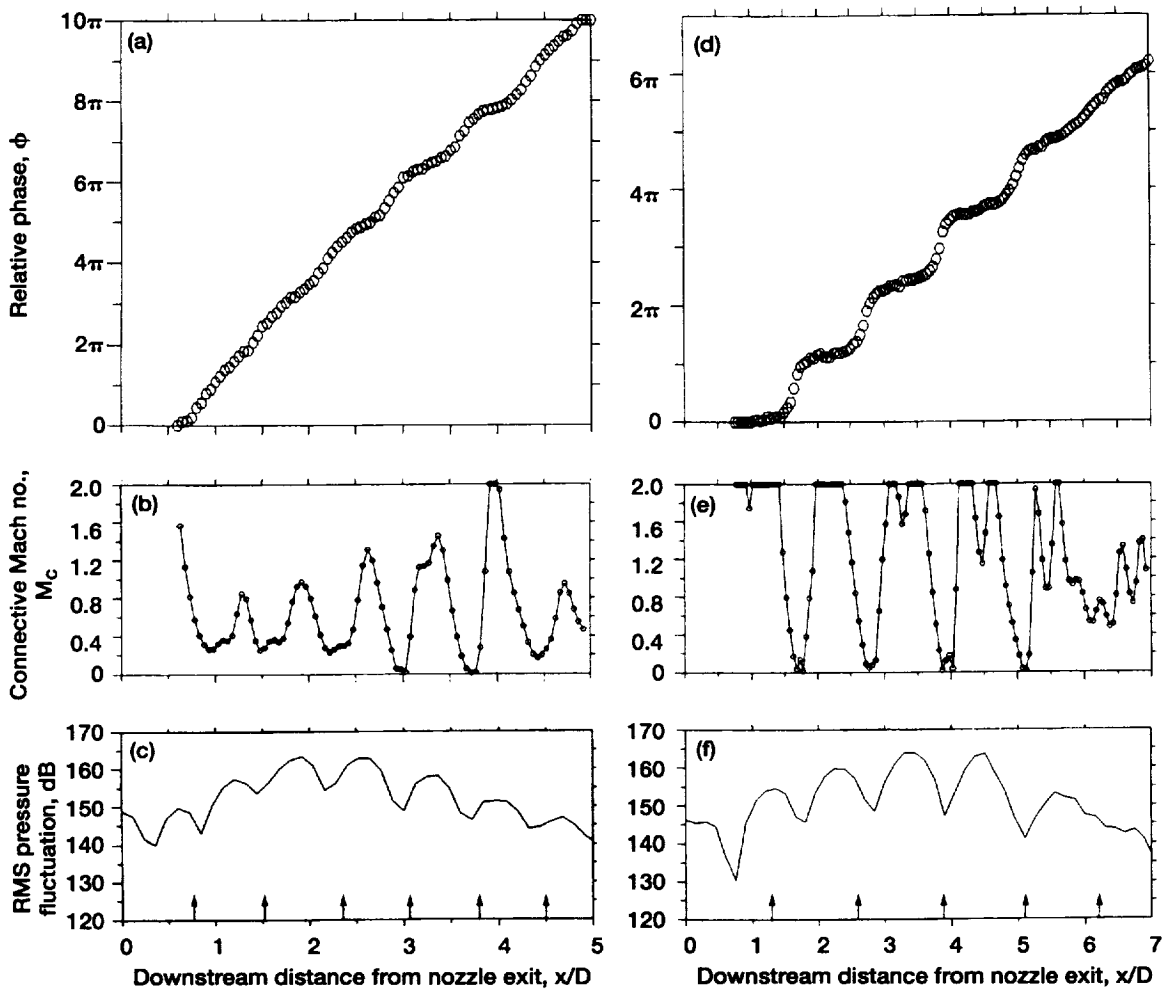


Figure 13.—Phase, convective Mach number, and rms pressure fluctuations just outside the boundary of (a), (b), (c) $M_j$ = 1.19, and (d), (e), (f) $M_j$ = 1.42 jet. Relative phase values are from cross-spectra of a fixed and a traversing microphone signals. The vertical arrows in (c) and (f) are shock locations.

National Aeronautics and
Space Administration

**Lewis Research Center**
21000 Brookpark Rd.
Cleveland, OH 44135-3191